Physics – Uspekhi **49** (4) 369 – 388 (2006)

REVIEWS OF TOPICAL PROBLEMS PACS numbers: 61.50.Ks, 61.66.Bi, **62.50.+p**

Simple metals at high pressures: the Fermi sphere – Brillouin zone interaction model

V F Degtyareva

DOI: 10.1070/PU2006v049n04ABEH005948

Contents

Abstract. High-pressure structural transformations are analyzed for simple sp-elements and some binary alloys. The crystal structure stability of these metals depends on the Fermi surface – Brillouin zone interaction. An increase in this interaction with pressure results in transitions to less symmetric and less closely packed structures. A structural similarity is shown to exist between the high-pressure phases for alkali and alkali-earth metals and for polyvalent group IV and V elements. The correlation between the behavior under compression of the structure and the physical properties (resistivity and superconductivity) of these metals is discussed in terms of the Fermi sphere – Brillouin zone interaction model.

1. Introduction

The study of the structure and properties of substances at high pressure is needed to understand the physical processes that take place in a highly compressed state, in which a large fraction of matter in the universe exists. In the last decade substantial progress has been achieved in analyzing the structure of matter under pressure thanks to the constant improvement in the methods of investigation (synchrotron radiation, high-resolution image plate detector, diamond anvils operating in the megabar pressure range, and single-crystal samples). This progress has led to interesting and unexpected results when the crystal structure of the high-pressure phases of a number of elements is investigated. Among the most vivid examples are

• the complex orthorhombic structure *oC*16-*Cmca* for Cs-V and Si-VI [1, 2];

• the low-symmetry cubic structure *cI*16 for lithium [3];

• complex polyatomic structures *oC*84 for Cs-III [4] and *oC*52 for Rb-III [5];

• incommensurate host – guest structures for the group II elements Ba [6] and Sr [7], for the group V elements Bi, Sb, and As [8, 9], and for the group I element Rb [10, 11]; and

• incommensurately modulated structures for the group VII element I [12] and for the group VI elements Te, Se, and S [13, 14].

These discoveries have forced researchers to reconsider the common idea that pressure assists the transition of matter to more compact, high-symmetry structures. But what are the physical reasons for the formation of low-symmetry, non-compact structures in simple (sp) metals at high pressure? In this connection it is advisable to compare the new data on the crystal structure of elements with the earlier data on their electrophysical properties (electric conductivity and superconductivity) in the compressed state.

Of special interest are alkali and alkali-earth metals, in which pressure-induced unusual transformations to phases with various, often unpredictable, structures have been discovered. These transformations are related to the non-monotonic variation of electrical resistivity and to the emergence of superconductivity. The observed general nature of the structure types under pressure for group I and II elements and polyvalent elements of groups IV and V merits special attention and discussion, since it suggests a similarity

V F Degtyareva Institute of Solid State Physics,
Russian Academy of Sciences,
142432 Chernogolovka, Moscow Region, Russian Federation
Tel. (7-496) 993-27 55. Fax (7-496) 524-97 01
E-mail: degtyar@issp.ac.ru

Received 17 February 2005, revised 25 October 2005
Uspekhi Fizicheskikh Nauk **176** (4) 383 – 402 (2006)
Translated by E Yankovsky; edited by M V Magnitskaya

between the states of the valence electrons of these metals. The behavior of elements at high pressure has been recently discussed in a number of review articles (see Refs [15 – 18]). However, experimental studies in this field constantly supply new data, which need to be generalized and systematized.

In the present article we examine the structural transformations that take place in simple metals under pressure using the concept of the interaction between the Fermi sphere and the Brillouin zone within the nearly free electron model, which holds for s- and sp-metals. The stability of the crystal structure of metals is known to be determined by two main energy terms: the electrostatic contribution of ions, $E_{\text{el. st.}}$ (the Madelung energy), and the band structure energy of valence electrons, E_{band}. A theoretical description of the energy of the crystal can be found in textbooks and monographs (e.g., see Refs [19 – 22]). If we want to have a qualitative understanding of the structural transformations that take place under pressure, we must note that the two main contributions to the energy of the crystal, $E_{\text{el.st.}}$ and E_{band} depend on the volume differently (as $V^{-1/3}$ and $V^{-2/3}$, respectively). This fact determines the change in the balance between the energy contributions as the pressure increases in favor of the electron contribution. At normal conditions what prevails is the electrostatic contribution, which in metals stabilizes the close-packed, high-symmetry structures, to which the face-centered cubic (fcc), hexagonal close-packed (hcp), and body-centered cubic (bcc) structures belong. When metals are in a compressed state, the band contribution of valence electrons grows, and the crucial factor in reducing the energy of the crystal structure is the emergence of faces of the Brillouin zone near the Fermi level. This leads to the formation in metals of low-symmetry complex structures with reduced compactness and lower coordination numbers,

The decisive role that valence electrons play in structural stability manifests itself in binary alloys of sp-metals at normal pressure. In Sections 2 and 3 we discuss the phases in Cu – Zn alloys and in In- and Sn-based alloys. The selected binary alloys are formed by components that are neighbors in the periodic table and have close atomic radii, similar electron configurations, and a minimum difference in electronegativity, which suggests the formation of broad regions of solid solutions. Such binary alloys can be considered a 'model element' with a varying number of valence electrons fixed by the alloy's composition. Analysis of the structure of phases in such systems makes it possible to establish the importance of the contribution of the valence electrons for the formation of the structure, and it is assumed that other contributions are insignificant. The study of alloys as metals with varying valence becomes especially important if we want to understand the high-pressure phases of pure elements in connection with the overlap of electron levels and with changes in the number of electrons in the valence band under strong compression.

2. A prototype of a system with Hume-Rothery phases: the Cu – Zn system

The important role that the contribution of valence electrons plays in the formation of the crystal structure of metals and alloys manifests itself most vividly in binary phases based on noble metals, which are known as Hume-Rothery phases. The Cu – Zn system is a classical example of a system with Hume-Rothery phases, a system exhibiting a sequence of phases with the structures fcc – bcc – complex cubic – hcp, which are called the α-, β-, γ-, and ε-phases, respectively. Hume-Rothery was the first to notice [23] that the same sequences of phases exist in other binary systems where one component is a metal of the copper group and the other is a polyvalent element of the II – V groups (Zn, Cd, Al, In, etc.). The regions in which such phases exist are determined by the average number of valence electrons per metal atom, or the electron concentration z, while the valence of each component is assumed equal to the number of the group.

Mott and Jones [24] used the Fermi sphere – Brillouin zone interaction model to explain the stability of Hume-Rothery phases. As the electrons move in the periodic field of a crystal, there opens an energy gap in the vicinity of the Brillouin zone face, $q = 2k_{\text{F}}$, which lowers the electron energy. A structure for which the gain in the electron energy is greater thanks to the Fermi sphere – Brillouin zone interaction is a more favorable one. The Fermi momentum in the nearly free electron model is defined as the radius of the Fermi sphere: $k_{\text{F}} = (3\pi^2 z/V)^{-1/3}$, where z is the number of valence electrons per atom and V is the atomic volume. The condition $k_{\text{F}} = q/2$ yields the quantitative definition of the limit of stability for a Hume – Rothery phase as a function of composition z varying from 1.36 for fcc to 1.48 for bcc.

The complex cubic structure of gamma brass in Cu – Zn alloys is an example of such a phase, in which at normal conditions the electrostatic contribution loses the 'battle' with the electron contribution, so that the key factor in the structure's stability is the Fermi sphere – Brillouin zone interaction. The structure of Cu_5Zn_8 has the space group $I\bar{4}3m$ and 52 atom per unit cell (the Pearson symbol is $cI52$) [25]. This structure is considered a derivative of bcc with a triple period $3 \times 3 \times 3$ and the removal of two atoms. In the new cell the atoms are slightly displaced from the bcc positions so that the interatomic spacings become equal, which leads to the appearance of a new structural reflection (411) with the same spacing as the (330) reflection. As a result, in the Brillouin – Jones zone for gamma brass there appear 24 new planes in addition to the 12 planes in the Brillouin zone for bcc, as shown in Fig. 1a. Here and in what follows, for complex structures we take large zones, or Brillouin – Jones zones, whose planes lie near the Fermi surface, but will call them, for the sake of brevity, Brillouin zones. According to an estimate of the ratio $V_{\text{F.s.}}/V_{\text{B.z.}}$ in the nearly free electron model, the extent to which the Brillouin zone of gamma brass is filled with electron states amounts to roughly 93%.

The main components of Hume-Rothery effects become obvious if we turn to the example of the structure of gamma brass:

- the Brillouin (or Brillouin – Jones) zone is formed by planes that emerge near the Fermi surface and have a strong structure factor, and
- the shape of the Brillouin zone is that of a symmetric polyhedron with many faces, which accommodates very well the Fermi sphere, with high filling of the Brillouin zone by electron states.

In Section 4 we will discuss how the enhancement of Hume-Rothery effects manifests itself in alkali metals under pressure. Here, we will briefly discuss the behavior of the brass phases in the Cu – Zn system at high pressures. In a recent study of the structures of alpha, beta, and gamma brass in the Cu – Zn system [25], the pressure was raised to 50 GPa. The gamma brass phase proved to be stable up to this pressure, while for the alpha and beta phases the onset of transformations into other, more complex, phases was

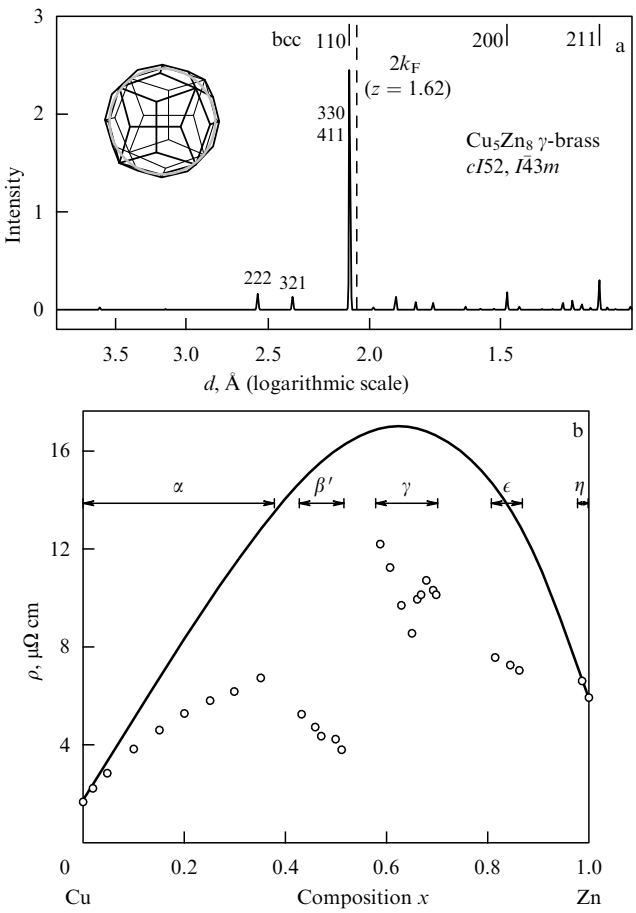

Figure 1. (a) Diffraction pattern of the gamma brass Cu_5Zn_8 (the $cI52$ structure) with a strong structural maximum (330) + (411) near $2k_F$; the inset shows the Brillouin zone with the planes (330) and (411) and the Fermi sphere with the radius $k_F = (3\pi^2 z/V)^{1/3}$ for $z = 1.62$ (the values of the interplanar spacing d are shown on the logarithmic scale). (b) Electrical resistivity of Cu – Zn alloys as a function of composition. The solid curve represents the concentration dependence in the virtual crystal model (taken from Ref. [27]).

discovered at 20 and 37 GPa, respectively. What is interesting is that the stability of brass phases correlates to the filling of the Brillouin zone, equal to 0.62, 0.75, and 0.93 for the α-, β-, and γ-phases, respectively. The pressure-induced transition of fcc and bcc phases into complex structures and the stability of gamma brass up to 50 GPa correspond to the tendency of enhancement of Hume-Rothery effects as metals are compressed.

Note that the electrophysical properties of the phases in the Cu – Zn system at normal pressure vary with composition in a nonmonotone manner [27]. Higher values of electrical resistivity have been obtained for gamma brass, as shown in Fig. 1b. Qualitatively, such dependence of the electrophysical properties on phase composition can be explained by the filling of the Brillouin zone by electron states, which is much higher in the gamma phase than in the alpha or beta phase. The filling of the Brillouin zone determines the configuration of the Fermi surface and provides a qualitative estimate of the size of the sections of the Fermi surface, which determine such properties as conductivity. We will use this qualitative dependence manifesting itself for Hume-Rothery phases in alloys at normal pressure, for phases of simple s-metals in a discussion of the electrophysical properties of alkali and alkali-earth metals under pressure.

3. The fcc – bcc structural transition in indium- and tin-based alloys

In- and Sn-based alloys with a tetragonal phase close to fcc and bcc present a good example of the key role that valence electrons play in the formation of the structure of metals. The cubic structures fcc and bcc can be considered on the basis of a general body-centered tetragonal (bct) cell with two atoms. The transition from fcc to bcc can be achieved by compressing bct along the c axis, as a result of which the c/a ratio changes from $\sqrt{2}$ to 1. Such an fcc – bcc transition was examined by Bain [28] in order to analyze the structure of martensite and became known as a Bain path. Under normal conditions iron is known to have a bcc structure, while at temperatures above 911 °C it has an fcc structure. When low-carbon steel is quenched, austenite (fcc) transforms into martensite, a phase with a bct structure that is a solid solution of carbon in iron.

The fcc – bcc transformations have been observed in a number of elements when temperature or pressure is raised [29, 30]. Tetragonal phases appear in metals when thin films are deposited on a substrate and are caused by the dimensional mismatch between the film atoms and the substrate atoms, a phenomenon known as epitaxial Bain path [31].

In the cases we have just considered the transformations related to the fcc – bcc transition are caused by external factors such as temperature, pressure, or strain. In this section we discuss tetragonal phases between fcc and bcc, phases whose stability is related to an internal factor, the number of valence electrons per atom in the metal. We analyze the crystal structure of the phases in indium- and tin-based binary alloys existing at normal conditions and also forming under high pressure. We also examine the general dependence of the extent of tetragonal distortion (the c/a ratio) on the alloy's composition, which is characterized by the electron concentration (the average number of valence electrons per atom of the metal) and discuss the reasons for this dependence within the Fermi sphere – Brillouin zone interaction model.

3.1 Why is indium tetragonal? Tetragonal phases in indium alloys at normal and high pressure

In the periodic table the boundary between metals and nonmetals passes along group III – IV elements. In group III, the lightest metal, aluminum, crystallizes into an fcc structure, while the heavier metal indium has a tetragonally distorted fcc structure slightly extended along the c-axis. The crystal structure of indium is described as bct with the space group $I4/mmm$, the Pearson symbol $tI2$, two atoms per unit cell located at (0, 0, 0) and (1/2, 1/2, 1/2), and $c/a = 1.521$. Since the structure of indium it close to fcc, it has proved convenient to describe it as face-centered tetragonal (fct) with four atoms per cell and $c/a = 1.076$ [25].

High-pressure studies of indium have shown that the axis ratio c/a increases with pressure, reaches its maximum $c/a = 1.088$ at $P = 7$ GPa, and decreases under a further increase in pressure [32]. It could be expected that at even higher pressures the c/a ratio approaches unity and the structure of indium becomes cubic. However, studies at pressures up to 93 GPa showed that no such transition occurs, that indium remains tetragonal up to roughly 45 GPa, and then its structure becomes more complex, presumably orthorhombic [33].

For a lighter group III element, gallium, the structure at normal conditions is complex orthorhombic; Ga becomes

similar to In as the pressure grows, assuming the fct structure at $P > 12$ GPa, which then transforms into the fcc structure (at $P > 120$ GPa) [34]. Theoretical calculations for In and Ga done by Simak et al. [35] confirm the presence of an energy minimum for tetragonal structures at $c/a \sim 1.52$ under compression. What is interesting is that these calculations reveal the presence of a second, more shallow, minimum near $c/a \sim 1.32$. The tetragonal phase with such a value of c/a is not implemented for pure indium and gallium but is formed when In is alloyed with Sn and Pb.

3.1.1 Variations in c/a for phases in indium alloys at normal pressure. Variations in the tetragonality of indium occur when indium is alloyed with metals that are neighbors of In in the periodic table, with which In forms broad regions of solid solutions [36]. The alloying of indium with the divalent metals cadmium or mercury causes a decrease in c/a, and 6 at.% of Cd or Hg makes the structure cubic (fcc). The alloying of indium with the tetravalent metals tin or lead increases the value of c/a of the tetragonal structure. However, when the alloy has more than 13 at.% of Sn or Pb, the axial ratio for the fct structure suddenly drops from $c/a > 1$ to $c/a < 1$.

The observed variation in tetragonality for phases in indium-based alloys caused by variations in the composition of the alloys points to a correlation between c/a and the average number of valence electrons in the alloy per atom of the metal, or the electron concentration z. Figure 2 presents the data for tetragonal phases in In-based alloys, known for normal conditions [37]. It depicts the dependence of c/a on the electron concentration z, in calculating which the valence of the metal is assumed equal to the number of the group in the periodic table.

Svechkarev [38] suggested an explanation of the dependence of the tetragonal distortion for phases in indium alloys on the composition. He examined the condition needed for the Fermi sphere to touch the Brillouin zone at the points W and W′, with the result that the electron energy has a minimum. A tetragonal distortion of a cubic lattice occurs because of the splitting of the reciprocal lattice vectors (200), which is related to the Fermi sphere touching the vertices W′ ($c/a > 1$) or W ($c/a < 1$) of the Brillouin zone, as shown in Fig. 2. The importance of the effects associated with such touching of the Fermi sphere and the Brillouin zone for certain axial ratios to set in for In-based structures has been noted by Heine [22].

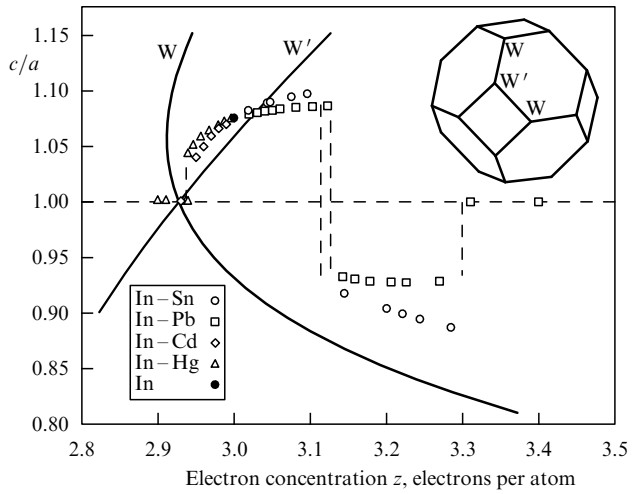

Figure 2. Face-centered tetragonal (fct) phases in In-based alloys at normal pressure (the data was taken from Pearson's handbook [37]). Shown is the dependence of c/a of the phases on the alloy composition, the electron concentration z. The solid curves represent the calculated condition needed for the Fermi sphere with the radius corresponding to the given z to touch the Brillouin zone for the fct structure at points W or W′ (from Svechkarev's paper [38]). The Brillouin zone for the fcc structure is shown in the upper right corner.

At present, interest in the problem of tetragonal structures of the indium type is growing and a new direction of high-pressure research is establishing itself. A number of studies involving indium alloys have shown that Fermi sphere – Brillouin zone effects become more pronounced as the pressure increases and provide new proof of the validity of Svechkarev's proposition.

The models of nearly free electrons and Fermi sphere – Brillouin zone interaction can be used for sp-metals and In-, Cd-, and Sn-based alloys. The valence state does not change as the pressure increases, so that structural changes caused by compression should be attributed solely to the strengthening of the electron interaction compared to the electrostatic contribution. This manifests itself in a tetragonal distortion of the fcc lattice of the alloys and in an increase in this distortion with pressure, as shown in our studies of alloys under pressure, described below.

On the other hand, by applying high pressure it is possible to produce new structural states of elements and alloys, which broadens the experimental base of theoretical models. For instance, the group IV element Sn transforms under pressure into a bct structure close to bcc, with $c/a \sim 0.95$. The tetragonality of this structure changes under alloying of tin with lower valence elements (In and Hg) in alloys under high pressure. This family of tetragonal phases with a structure of the bct-Sn type is discussed in Section 3.2.2.

Both families, fct-In and bct-Sn, are discussed in Section 3.3, where a generalized picture for tetragonal phases from fcc to bcc reflecting the dependence of c/a on the electron concentration z is presented. At the end of Section 3 we examine the possibility of using the Fermi sphere – Brillouin zone interaction model, which operates well for sp-metals and alloys, in cases of tetragonal phases in elements and compounds with a varying number of valence electrons at high pressure.

3.1.2 Tetragonal phases in indium alloys at high pressure. An interesting problem concerning indium alloys was that of the stability of cubic phases at high pressure. To solve it, alloys with an fcc phase in In – Cd and In – Pb alloys were chosen. An unexpected result of this research was the transition under pressure from the cubic phase to the tetragonal. What was interesting was the dependence of c/a for tetragonal phases on the alloy composition, or the electron concentration z.

The fcc – fct transition in In *alloys*. The phase with the fcc structure forms in In – Cd alloys with ~ 6 at.% Cd. The initial alloy In – 10 at.% Cd contained the fcc phase and a small amount of hcp-Cd, in accordance with the well-known phase diagram [36]. As the pressure is raised to 1.4 GPa, the fcc – fct transformation takes place, apparently without any changes in composition in these phases, since the additional hcp-Cd phase is retained [39]. The tetragonal structure of In – 6 at.% Cd remains stable up to roughly 30 GPa, with c/a increasing from 1.04 to 1.07. As the pressure is lowered, the reverse fct – fcc transformation takes place, and at normal pressure the alloy returns to its initial state. The variation of the axial ratio for the In – 6 at.% Cd phase from 1 to 1.07 is shown in Fig. 3a

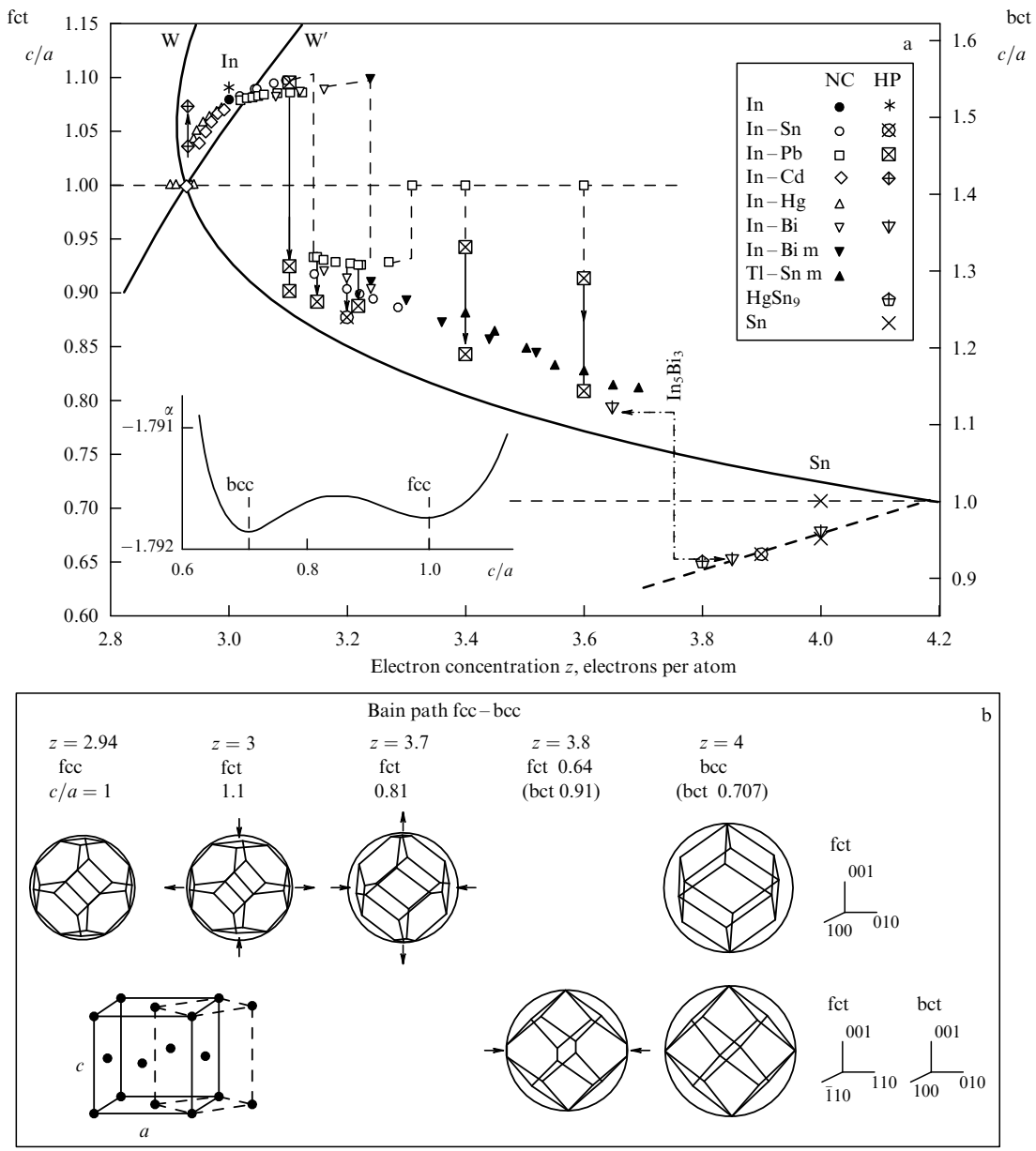

Figure 3. (a) Generalized diagram of the dependence of c/a on z for tetragonal phases in indium and tin alloys for the fcc – bcc Bain path; the data for the phases, stable and metastable (m), under normal conditions (NC) have been taken from Ref. [37], while the data for the phases under high pressure (HP) have been taken from Refs [39, 40, 43 – 46]. The solid curves represent the condition needed for the Fermi sphere to touch the Brillouin zone. The inset in the lower left corner shows the dependence of the Madelung constant α on c/a for the tetragonal phases, with the two minima corresponding to the cubic structures fcc and bcc. (b) The fcc – bcc Bain path and the Fermi sphere – Brillouin zone interaction model. Depicted are the changes in the configuration of the Brillouin zones caused by an increase in the radius of the Fermi sphere in accordance with the increase in z, with the Fermi sphere and Brillouin zone still in contact.

for the corresponding value $z = 2.94$. At this value of z the curves W and W' calculated from the condition needed for the Fermi sphere and the Brillouin zone to touch intersect. Under pressure the phase for which c/a approaches curve W becomes stable.

The phase with the fcc structure exists in In – Pb alloys within a broad range of compositions from 30 to 100 at.% Pb, in accordance with the well-known phase diagram (see Ref. [36]). Alloys with 40 and 60 at.% Pb were selected for the research at high pressure. These alloys have an fcc phase with lattice periods equal to 4.834 and 4.868 Å, respectively. High-pressure studies of indium alloys with 40 and 60 at.% Pb have revealed that the cubic phase transforms into the fct phase at pressures above 3 and 10 GPa with c/a suddenly decreasing from 1 to 0.94 and 0.92, respectively [39]. Tetragonal distortion grows with pressure and at 36 GPa reaches values of 0.85 and 0.81 for the phases with 40 and 60 at.% Pb, respectively. The fcc – fct transformation in these alloys is reversible, and the initial fcc phase is restored when the pressure is decreased. The observed variation of c/a in the phases of In – 40 at.% Pb and In – 60 at.% Pb are shown in Fig. 3a for the corresponding values of z, equal to 3.4 and 3.6. Obviously, as the pressure grows the value of c/a decreases from 1 to values that approach the Svechkarev diagram, i.e., the curve W on the condition that the Fermi sphere and the Brillouin zone touch.

Variation in c/a in the tetragonal phase of the $In_{90}Pb_{10}$ *alloy from $c/a > 1$ to $c/a < 1$.* The observed dependence of c/a on z

for tetragonal phases in indium alloys and the established tendencies in the variation in c/a with pressure made it possible to suggest that near the critical concentration $z = 3.12-3.15$ of electrons per atom there could be a special type of transformation. Under normal pressure in this range of compositions, the tetragonal distortion changes from $c/a > 1$ to $c/a < 1$. It was assumed that for alloys, whose composition is near the critical concentration, pressure inflicts structural changes characterized by a jump in c/a. For studies we used In – Pb alloys with 10, 15, and 20 at.% Pb. As the result of high-pressure structural research [40] it was found that the In – 10 at.% Pb alloy undergoes a transformation from one tetragonal phase to another tetragonal phase and that in the process the axial ratio changes from $c/a > 1$ to $c/a < 1$. In Fig. 3a this transition reveals itself by a jump in c/a at $z = 3.10$. Within a certain range of pressures there are two coexisting phases with different values of c/a, and the two-phase region is retained after prolonged annealing of the alloy at 11.3 GPa and 150 °C over the course of 18 h. This is an indication that the transition from an fct structure with $c/a > 1$ to an fct structure with $c/a < 1$ is a first-order transition rather than a consequence of kinetic processes. The transformations in the In – 10 at.% Pb alloy are reversible, and as the pressure decreases they proceed in the reverse order with a certain hysteresis in pressure.

Under normal pressure, the indium alloys with 15 and 20 at.% Pb crystallize in the fct phase with $c/a < 1$. As the pressure grows, the tetragonality of the phase increases, i.e., c/a decreases. At $P \sim 30$ GPa the value of c/a for such a phase approaches the calculated curve that represents the condition that the Fermi sphere touches the Brillouin zone, as shown in Fig. 3a for values of z equaling 3.15 and 3.20, corresponding to the indium alloys with 15 and 20 at.% Pb, respectively.

High-pressure studies of In – Pb alloys near the critical composition region, within which at normal pressure there is a jump from $c/a > 1$ to $c/a < 1$ for the fct phases, showed that pressure raises the stability of the tetragonal phases for which the value of c/a approaches the calculated curve that represents the condition that the Fermi sphere touches the Brillouin zone at points W. The transition to the fct phase accompanied by a jump from $c/a > 1$ to $c/a < 1$ was predicted by the present author as a result of an analysis of the transformations of tetragonal phases in indium alloys under pressure and was corroborated by experiments. The structural variations in the tetragonal phases in In – Pb alloys within the critical region support the validity of Fermi sphere – Brillouin zone interaction model.

3.2 Tetragonal body-centered phase in tin and tin-based alloys

The Bain path describes the mechanism of transformation between the fcc and bcc structures. Above, we examined the tetragonal phases that are close to fcc, the fcc – fct transformation, and the transition from the fct phase with $c/a > 1$ to the fct phase with $c/a < 1$. Here, we discuss the phases with a bcc structure and the tetragonal phases that are close to bcc and form at high pressure in tin and tin-based alloys. In the case at hand the high pressure is a tool for producing metallic phases that do not exist at normal pressure, which makes it possible to broaden the general picture of structural states of metallic phases in the range of electron concentrations from 3 to 4 and to follow the complete cycle of fcc – bcc variations.

3.2.1 High-pressure bct and bcc phases for Sn and InBi. In normal conditions, tin has the tetragonal structure of white tin with four atoms per cell, *tI*4. Olijnyk and Holzapfel [41] studied Sn under pressure and found that at pressures higher than 10 GPa Sn acquires a bct structure with two atoms per cell, a structure that is close to bcc, with $c/a < 1$. As the pressure grows, the tetragonality decreases from 0.912 to 0.955, thus approaching 1. However, the bcc – bct transition occurs discontinuosly at pressures above 35 GPa. Within a certain pressure range (from 35 to 45 GPa), the two phases, bct and bcc, coexist, which indicates that the bct – bcc transition is of first order. In Figure 3a, the bcc and bct phases for Sn are indicated for $z = 4$.

For a long time the bct-Sn structure remained unique, raising questions about the reasons for tetragonal distortion in the bcc structure. Theoretical calculations yield fairly close values of energy for tin in the bct and bcc structures, which makes it impossible to determine the order in which these structures emerge as the pressure is varied [42]. The Fermi sphere – Brillouin zone interaction model provides a qualitative understanding of the energy contributions that lead to tetragonal distortions of the cubic structure and makes it possible to quantitatively describe c/a as a function of the electron concentration z for the bct phase produced at high pressure for the compound InBi, which is isoelectronic to Sn ($z = 4$) [43], and for the alloys Sn – 20 at.% In and Sn – 10 at.% Hg ($z = 3.8$) [44, 45].

The compound InBi belongs to the class of semiconducting compounds $A_{\mathrm{III}}B_{\mathrm{V}}$ but differs in structure from compounds with lighter components. Such compounds as InSb, GaSb, and InAs have a diamondlike cubic structure of the ZnS type with tetrahedral coordination. However, in normal conditions InBi crystallizes in a tetragonal structure of the PbO type with four atoms per cell and an axial ratio $c/a = 0.95$. At pressure higher than 7 GPa there is considerable compression along the c-axis: the value of c/a suddenly drops to 0.61. As the pressure becomes higher than 20 GPa, the tetragonal structure of the alloy becomes body-centered and disordered, i.e., indium and bismuth atoms occupy the positions (0, 0, 0) and (1/2, 1/2, 1/2) with equal probability. Such a phase corresponds to the *tI*2 with $c/a = 0.91$ and is identical to bct-Sn. In contrast to tin, the bct-InBi phase is stable up to higher pressures, and the bct – bcc transition begins in InBi at ~ 70 GPa [43]. The value of c/a for bct-InBi first rapidly increases with pressure, but at $P > 40$ GPa it saturates, reaching its maximum value $c/a = 0.96$, which is close to the maximum of c/a for bct-Sn, as shown in Fig. 3a for $z = 4$. Such behavior of bct-InBi and bct-Sn under pressure and a sudden transformation to the bcc phase suggested that the general reason for the tetragonal distortion of the bcc structure is the isoelectronic structure of these substances (the average number of valence electrons per cell $z = 4$). The assumption has been corroborated in high-pressure studies of Sn alloyed with In and Hg, where the average valence of the metal atoms in the alloy is lower.

3.2.2 The bct phase in Sn – In and Sn – Hg alloys. In the binary systems Sn – In and Sn – Hg at normal pressure there exists a phase with a simple hexagonal structure *hP*1 at 20 at.% In and 10 at.% Hg, in accordance with the well-known phase diagrams (see Ref. [36]), which corresponds to $z = 3.8$. The *hP*1 structure consists of close-packed hexagonal layers stacked according to the sequence AAA... with an axial ratio for the hexagonal cell close to 1 ($c/a = 0.93$). Interest

in studies of alloys with the $hP1$ structure under pressure stemmed from the discovery of such a structure in the group IV elements Si and Ge subjected to high pressure [30]. Under a further increase in pressure the phase $hP1$ in Si and Ge transforms into more closely packed structures (hcp or dhcp, double hcp) through the complex orthorhombic phase $oC16$-$Cmca$. Studying the chain of transformations under pressure for the $hP1$ phase in Sn-based alloys has also been of interest.

Research in this field showed that the phase $hP1$ in Sn alloys remains stable up to about 10 GPa, while at higher pressures this phase transforms to bct, which is a solid solution of In or Hg based on bct-Sn. The bct phase exists in Sn – In and Sn – Hg alloys at pressures up to 20 and 60 GPa, respectively, while at higher pressures one more phase, with an hcp structure, exists in the alloys of the given compositions [44, 45]. The results for the bct phase in Sn alloyed with Hg make it possible to follow the variations in c/a within a broad range of pressures from 13 to 60 GPa. The bct-Sn(Hg) phase appears at $c/a = 0.907$, which grows to 0.919 at $P = 40$ GPa, and then remains practically the same as the pressure is raised to 60 GPa, above which pressure a second phase, hcp, begins to appear in the alloy.

Comparison of the limit values of c/a for the bct phase in pure tin and in InBi and for the bct phase in Sn(Hg) shows an increase in tetragonality from $c/a = 0.96$ for $z = 4$ to $c/a = 0.92$ for $z = 3.8$. These conclusions are corroborated by the data obtained for the Sn – 20 at.% In alloy for the bct phase, which exists at 16 – 21 GPa and for which c/a varies from 0.893 to 0.908. The explanation of the stability of the tetragonal phase in relation to the bcc phase and the obtained values of c/a for different values of z was done on the basis of the Fermi sphere – Brillouin zone interaction model when the Fermi sphere and the plane (200) of the Brillouin zone touch:

$$\text{from the condition } \frac{2\pi}{a} \leqslant k_{\mathrm{F}} \text{ follows } \frac{c}{a} \leqslant \frac{3}{4\pi} z\,.$$

Such an estimate yields $c/a \leqslant 0.96$ for $z = 4$ (Sn, InBi) and $c/a \leqslant 0.92$ for $z = 3.8$, which was corroborated in experiments involving Sn – 10 at.% Hg and Sn – 20 at.% In alloys [44, 45].

3.3 Generalized diagram of tetragonal phases for the fcc – bcc deformation. The Fermi sphere – Brillouin zone interaction model and stability of tetragonal phases

Figure 3a shows a generalized picture for tetragonal phases in In- and Sn-based alloys, which reflects the variation in c/a from fcc to bcc as a function of z. The diagram combines the tetragonal fct phases that are close to fcc and the bct phases that are close to bcc.

The experimental substantiation needed for producing a collective diagram was obtained through studies of the compound In_5Bi_3 at high pressure [46]. The stoichiometric compound in the In – Bi system corresponding to the electron concentration $z = 3.75$ becomes unstable when the pressure exceeds 15 GPa and the temperature becomes $T = 150$ °C. The compound then decomposes into two phases with different compositions, which have the same bct structure but different values of c/a: the phase with $c/a = 1.126$ corresponds to the composition with ~ 34 at.% Bi ($z = 3.68$), and the phase with $c/a = 0.923$ corresponds to the composition with ~ 44 at.% Bi ($z = 3.88$), as shown in Fig. 3a. The results on the decomposition under pressure of In_5Bi_3 into two bct phases with $c/a > 1$ and $c/a < 1$ show that there exists a critical range of compositions near $z = 3.75$ where bct phases close to bcc undergo a jump from $c/a > 1$ to $c/a < 1$. In_5Bi_3 with $z = 3.75$ lands in the c/a discontinuity region, and this explains the decomposition of the compound under pressure into two tetragonal phases with different values of c/a and, correspondingly, with different values of z.

Earlier, we discussed the region of sudden variation in c/a for fct phases close to fcc from $c/a > 1$ to $c/a < 1$ near the compositions $z = 3.10 - 3.15$. Thus, as shown in Fig. 3a, there are three distinct regions in the dependence of c/a on z. In the middle of the diagram, from $z = 3.15$ to $z = 3.75$, the value of c/a monotonically decreases as z increases. However, as z approaches the fcc and bcc positions, there emerge critical regions (near $z = 3.15$ and $z = 3.75$) in which c/a undergoes a jump with the sign of the corresponding tetragonal distortion changing in the process.

3.3.1 The fcc – bcc deformation and the Fermi sphere – Brillouin zone interaction model. To explain the observed dependence of c/a on z, we must examine the balance of the two main energy contributions, i.e., the electrostatic energy and the energy of the electron band structure. The electrostatic contribution, expressed by the Madelung constant α, has two minima for the cubic structures fcc and bcc, as shown in the inset in Fig. 3a, with a small, shallow maximum between these minima [22]. When only the electrostatic contribution is taken into account, the fcc – bcc deformation is accompanied by a monotonic variation of c/a, as is the case in the middle region $z = 3.15 - 3.75$. The rapid variation in c/a outside this region, near the values of c/a for the fcc and bcc phases, should be attributed to the presence of the other contribution, the band structure energy, which is taken into account by the Fermi sphere – Brillouin zone interaction model.

When the composition of the alloys changes, an increase in z for structures corresponding to the phases of a given composition leads to an increase in k_{F}, which results in deformation of the Brillouin zone, as shown in Fig. 3b. Near $z = 3.15$ the conditions needed for the Fermi sphere to touch the Brillouin zone change: the points of contact W′ are replaced by the points of contact W (the upper row in Fig. 3b). In the region where $z > 3.75$, the structure is determined by the proximity of k_{F} to the planes of the Brillouin zone of type (200) of the bcc structure (the lower row in Fig. 3b). The 'attraction' of these planes to the Fermi sphere and the 'drawing' of the vertices of the Brillouin zone into the sphere determine the extent of tetragonal distortion of the bcc stricture. The mutual arrangement of the fct – bct structures is shown in the lower left corner of Fig. 3b.

Thus, the structural fcc – bcc transformation (the Bain path) is followed in In- and Sn-based alloys when the composition, or the number of valence electrons per metal atom in the alloy, changes, i.e., when internal parameter z changes. The dependence of c/a on z within the limits of this transformation is nonmonotonic: in the middle part c/a depends on z almost linearly, while in the regions close to fcc or bcc the c/a ratio undergoes a substantial deviation from linearity. The resulting dependence can be explained by the balance between the electrostatic and electron contributions.

The structural fcc – bcc transformation has been examined for sp-metals and alloys, the elements In and Sn, and the In- and Sn-based alloys with their neighbors in the periodic table (Cd, Hg, Pb, and Bi). A common idea for these elements and their alloys is that the behavior of the valence electrons in them resembles that in the nearly free electron model.

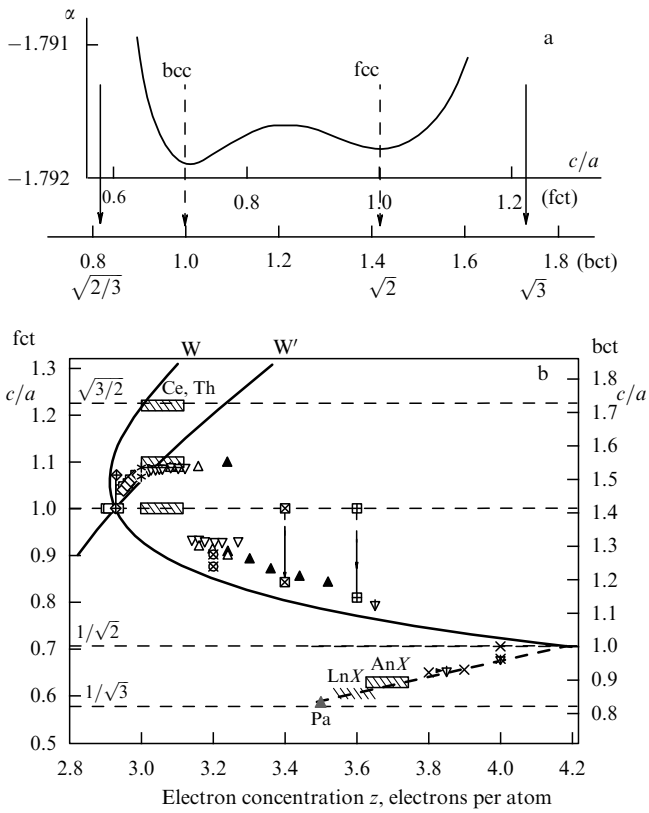

Figure 4. Extending the Bain-path model beyond the fcc–bcc transformation. (a) Solid arrows indicate the assumed minima in electrostatic energy in addition to fcc and bcc; the scale of c/a is given so that fct and bct can be compared. (b) Assumed positions of some lanthanide (Ce) and actinide (Th and Pa) phases and tetragonal pnictide phases on the curve of c/a as a function of z (the data on the structure of the phases and references are given in the main text). The horizontal dashed lines correspond to the minima of electrostatic energy depicted in Fig. 4a.

According to this model, the average number of valence electrons per atom (z) fixes the radius of the Fermi sphere $k_F = (3\pi^2 z/V)^{1/3}$, whose value determines the geometry of the Brillouin zone in such a way that the Fermi sphere – Brillouin zone interaction leads to a minimum value of the electron band structure contribution in conjunction with the electrostatic contribution.

Earlier we noted that there are two minimum values of the electrostatic energy in the series of bct structures corresponding to the transition from fcc to bcc, i.e., for $c/a = \sqrt{2}$ and 1. If we go beyond these values we see that there are other values of c/a at which minima in $E_{\text{el.st.}}$ can be observed (Fig. 4a). For instance, for the bct structure with $c/a = \sqrt{2/3} \approx 0.816$ there emerges an atomic configuration with the coordination number $N = 10$. On the other hand, for bct structures with $c/a = \sqrt{3}$ there emerges a special symmetry in the reciprocal space with the formation of regular hexagonal sections of the Brillouin zone for the case $\mathbf{q}_{101} = \mathbf{q}_{002}$. One can assume the tetragonal structures, with values of c/a at which the energy of the crystal structure is minimized thanks to two contributions, the electrostatic and the electron, to be especially stable.

3.3.2 Possible application of the Fermi sphere – Brillouin zone interaction model in analyzing the stability of tetragonal phases in rare-earth metals and actinides and their compounds. An interesting aspect of the above model is the possibility of using it to study tetragonal phases in metals with a complex configuration of valence electrons, say, in lanthanides and actinides and in some compounds with these metals. For this class of materials, we can try to describe the valence state by introducing an effective number of valence electrons that contribute significantly at the Fermi level.

The observed experimental values of c/a for the tetragonal phases of some lanthanides and actinides make it possible to determine their 'location' on the diagram representing the dependence of c/a on z and to estimate the corresponding 'effective' value of z. For instance, the bct structure of protactinium with $c/a = 0.825$ lands on the c/a diagram for bct phases of the Sn type near $z \sim 3.5$, which corresponds to partial delocalization of f-electrons in Pa (Fig. 4b). Clearly, at $c/a = 0.816$ bct-Pa is close to the electrostatic minimum. This is possibly the reason why the bct phase of Pa is especially stable at high pressures, and its axial ratio remains practically constant [47] up to 70 GPa.

A sequence of transformations under pressure accompanied by changes in the extent of tetragonal distortion of the cubic structure has been observed in cerium: the fcc structure (or the bct structure with $c/a = \sqrt{2}$) transforms into a body-centered monoclinic structure close to bct with $c/a = 1.52$ [48] and then into a bct with $c/a = 1.7$, which is stable up to 200 GPa [49]. The bct phases of cerium on the general diagram reflecting the z-dependence of c/a (Fig. 4b) occupy the position for $z = 3$, which corresponds to two branches at which the Fermi sphere touches the Brillouin zone at points W′ ($c/a = 1.52$) and W ($c/a = 1.7$). An fcc phase that is stable at a lower pressure corresponds to the minimum of electrostatic energy at $c/a = \sqrt{2}$. The Fermi sphere – Brillouin zone interaction effects stabilize the tetragonal phases at a higher pressure. Apparently, the additional contribution to the stability of the bct phase with $c/a = 1.7$ is caused by the proximity of the minimum of the electrostatic contribution at $c/a = \sqrt{3}$.

The above model describes a metal of the actinide group, thorium, in which the configuration of the valence electrons is similar to that of cerium. For thorium under pressure there is also an fcc – bct transformation with $c/a = 1.7$, and the bct phase remains stable up to approximately 300 GPa [50]. The stability of tetragonal phases in Ce and Th at high pressures is a manifestation of the special role of the electron contribution, while the c/a ratios for the bct phase are described by the Fermi sphere – Brillouin zone interaction model.

The above model provides an explanation for the high-pressure tetragonal phases for some lanthanide and actinide compounds and, in particular, for monopnictides, which are compounds of Ln and An with group V elements (As, Sb, and Bi). In normal conditions, these compounds have a structure of the NaCl type, but under pressure they transform into a more compact structure, a cubic structure of the CsCl type or a tetragonally distorted structure close to CsCl [51]. What is interesting is that the chalcogenides of Ln and An, compounds of these elements with group VI elements, form under pressure not a tetragonal structure but only a cubic structure of the CsCl type. This suggests that the electron factor plays a decisive role in the formation of tetragonal phases close to CsCl, assuming in these phases the formal value $z \sim 3.5$, which in the c/a vs. z dependence (Fig. 4b) corresponds to $c/a \sim 0.82$ that is observed in experiments involving LaSb and other compounds [51]. Thus, the model describing the dependence of c/a on the number of valence electrons and developed for simple sp-metals and alloys can be used to explain the stability of tetragonal phases in metals with a

complex configuration of the outer electron shells, e.g., in lanthanides and actinides, and also in some compounds based on these elements.

Finalizing this section, in which we discussed the crystal structure of indium and its alloys, we must mention the data on the structure and properties of the light elements of group III, boron and gallium, subjected to high pressure. The study of tetragonal phases in indium alloys at high pressures and the analysis of the pressure dependence of c/a make it possible to estimate the limits within which c/a varies for possible tetragonal phases of group III elements under compression. At present the crystal structure of metallic boron is not known, but the assumption is that complex structures known to exist for Ga at normal and high pressures and also bct structures of the indium type are formed. The Ga-II structure, stable at pressures from 2 to 10 GPa, has only recently been found to be orthorhombic with 104 atoms per cell, $oC104$ [52]. At higher pressures, Ga transforms to the bct phase similar to bct-In, and then to fcc. In the theoretical calculations involving boron [53] at high pressures, the fcc and bct structures with $c/a \sim 0.65-0.67$ are examined. Taking into account the good agreement between the data on tetragonal phases in indium alloys and the Fermi sphere – Brillouin zone interaction model, we can assume that boron is in the bct phase with c/a close to $\sqrt{2}$, as in the case of indium and gallium. Interest in the metallic state of boron stems from the discovery of superconductivity in this element at $P \geqslant 160$ GPa and $T_c = 4$ K, with an increase in T_c to 11 K at 250 GPa [54]. Changes in superconductivity with increasing T_c have also been observed for Ga: the orthorhombic phase of Ga at atmospheric pressure has $T_c = 1.09$ K, while for the Ga-II phase it has been found that $T_c = 6.4$ K at 3.5 GPa [55]. Note that for Ga the electrical resistivity in the complex phase $oC104$ increases compared to that of the bct phase of the indium type [56]. This suggests that the jump in resistivity in the transition to Ga-$oC104$ is caused by Hume-Rothery effects, which stabilize the low-symmetry complex structure under pressure. We discuss such changes in the electrophysical properties caused by the formation of high-pressure complex phases for alkali metals in the section that follows.

Li	7.5 39 42 55 60 67 bcc → fcc → $hR1$ → $cI16$ → orth1 → orth2 → orth3 < 85 GPa
Na	65 103 bcc → fcc → $cI16$ → (?) → (?) < 165 GPa
K	11.6 20 bcc → fcc → (host – guest) < 60 GPa
Rb	7 13 17 20 48 bcc → fcc → $oC52$ → (host – guest) → $tI4$ → $oC16$ < 70 GPa
Cs	2.4 4.2 4.3 12 72 bcc → fcc → $oC84$ → $tI4$ → $oC16$ → dhcp < 223 GPa
Ca	20 32 113 fcc → bcc → sc → complex (?) < 120 GPa
Sr	3.5 27 35 49 fcc → bcc → β-Sn, $tI4$ → $mI12$ → (host – guest) < 117 GPa
Ba	5.5 12 45 bcc → hcp → (host – guest) → hcp < 105 GPa

Si	12 13 16 38 42 80 $cF4$ → β-Sn, $tI4$ → $Imma$, $oI4$ → sh → $oC16$ → hcp → fcc < 250 GPa
Ge	11 75 85 102 160 $cF4$ → β-Sn, $tI4$ → $Imma$, $oI4$ → sh → $oC16$ → hcp < 180 GPa
Sn	0 8 45 $cF4$ → β-Sn, $tI4$ → bct → bcc < 120 GPa
Pb	13 110 fcc → hcp → bcc < 270 GPa
P	5 10 103 137 260 orth → $hR2$ → sc → complex (?) → sh → bcc (?) < 280 GPa
As	25 48 97 $hR2$ → sc → (host – guest) → bcc < 122 GPa
Sb	8 28 $hR2$ → (host – guest) → bcc < 65 GPa
Bi	2.5 2.7 7.7 $hR2$ → $mC4$ → (host – guest) → bcc < 220 GPa → $oC16$ (> 210 °C)

Figure 5. Sequences of structural transformations under growing pressure for group I and II elements and for group IV and V elements. The numbers above the arrows indicate the transition pressures in GPa.

4. Novel Hume-Rothery phases: alkali metals at high pressure

The sequences of structural transformations for alkali metals and alkali-earth metals are shown in Fig. 5. The data used in this figure were taken from Refs [30, 53, 57]. The most recent results were taken from the papers cited and discussed in the text. For the sake of comparison and discussion we also give sequences of structures under pressure for group IV and V elements.

4.1 Light alkali metals

For the simplest metal, the alkali element lithium, Ashcroft [58] predicted a complex behavior under pressure with the possibility of the valence electrons 'pairing' and a molecular phase forming. Recent structural studies of lithium under pressure revealed the formation of a complex cubic phase of lithium at pressures above 40 GPa [3]. The structure has 16 atoms per cell, the space group is $I\bar{4}3d$, and the Pearson symbol is $cI16$ (Fig. 6a). This structure can be considered a $2 \times 2 \times 2$ supercell of bcc with a small displacement of the positions of the atoms along the space diagonal. It is this displacement that leads to the formation of new structural reflections, and it is important to note that the reciprocal lattice vector for the first reflection (211) is close to $2k_F$, i.e., the planes (211) of the Brillouin zone lie almost on the Fermi sphere ($q_{211}/2 = k_F$). The general view of the Brillouin – Jones zone built for the (211) faces is shown in Fig. 6b (the data were taken from Refs [59, 60]). This high-symmetry polyhedron (tetragon-trioctahedron) with 24 planes accommodates the Fermi sphere very well with an electron state filling of roughly 90% (in the free electron model), which agrees with the conditions needed for Hume-Rothery phases.

The results of examining the Li-$cI16$ structure in the Fermi sphere – Brillouin zone interaction model suggest that the reason for the stabilization of this low-symmetry structure is the manifestation of Hume-Rothery effects, as in the case of gamma brass examined earlier. The energy of the crystalline phase lowers when the planes of the Brillouin zone form near the Fermi level and an energy gap opens in these planes. The Fermi sphere – Brillouin zone interaction effects modify the electron density of states with a substantial rise near (below) k_F and reduction directly at k_F.

Superconductivity in Li appears at $P > 20$ GPa, in the pressure range where the fcc phase is stable, reaches its maximum of 14 – 20 K and then decreases in a nonmonotone manner [61 – 63] (Fig. 7a). The electrical resistivity of Li

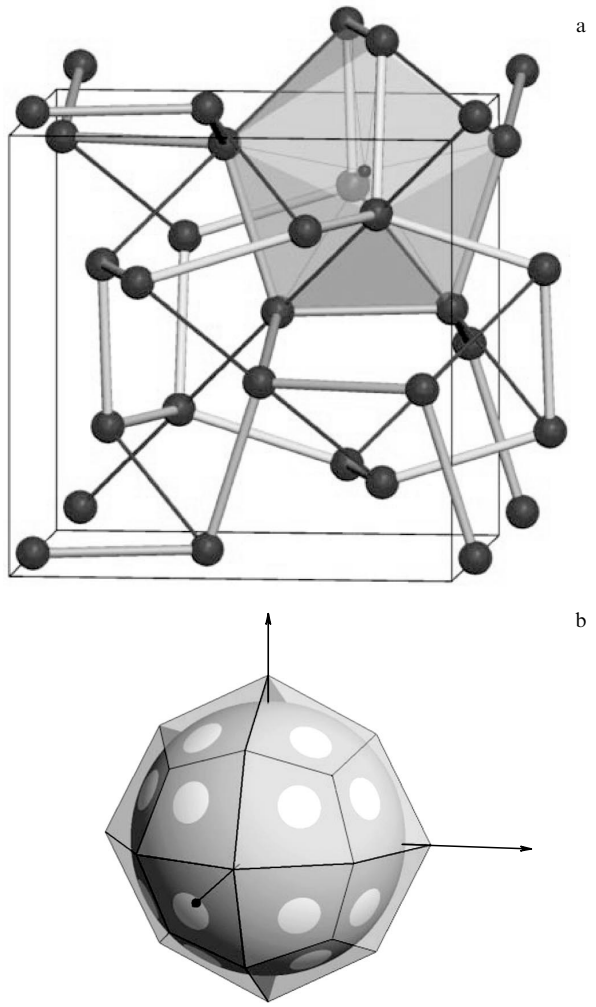

Figure 6. Lithium structure $cI16$ at 45 GPa. (a) Arrangement of atoms in the crystal cell (from Ref. [3]). (b) The Brillouin zone with (211) planes and the Fermi sphere for $z = 1$ (taken from Ref. [59]).

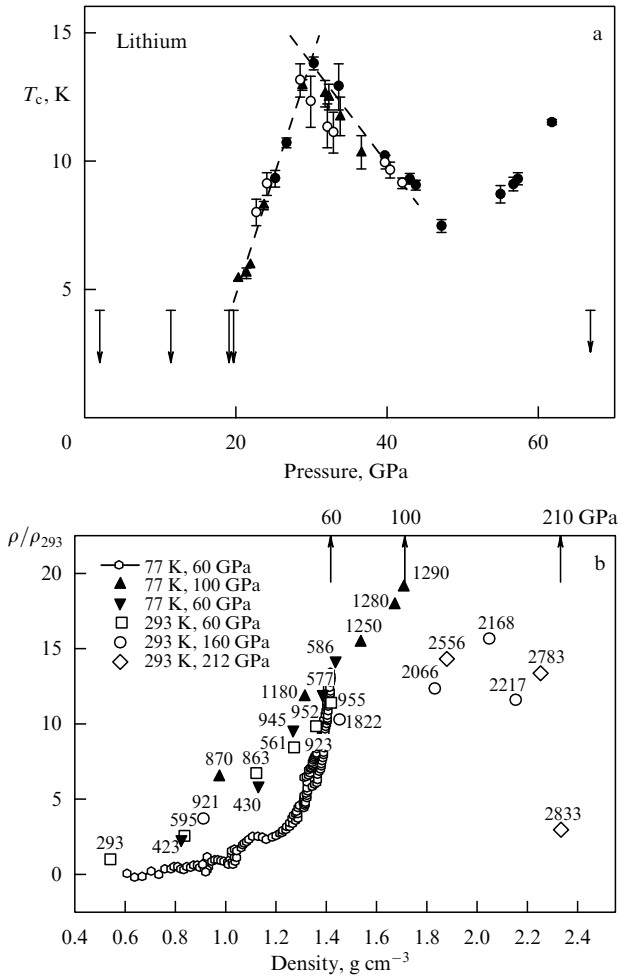

Figure 7. (a) Superconductivity of lithium under pressure (from Ref. [63]). (b) Resistivity of lithium as a function of density from multi-step shock-compression experiments. The initial temperature and maximum pressure are given for each group of measurements. The numbers near the points indicate the calculated temperature (from Ref. [65]).

increases with pressure. This was observed in research conducted with static compression [64] and dynamic loading [65] (Fig. 7b). The variation in the electrophysical properties of Li is significant already in the fcc phase and is caused by the enhancement of Hume-Rothery effects, which lead to a deviation of the Fermi surface from the spherical shape and to contact with the planes of the Brillouin zone, as shown in the theoretical calculations done in Refs [66] (Fig. 8).

The structure $cI16$ has also been found in sodium but at a higher pressure of about 130 GPa [16]. There is a certain similarity between the two light alkali metals, Li and Na, in the sequence of structural transformations, bcc – fcc – $cI16$.

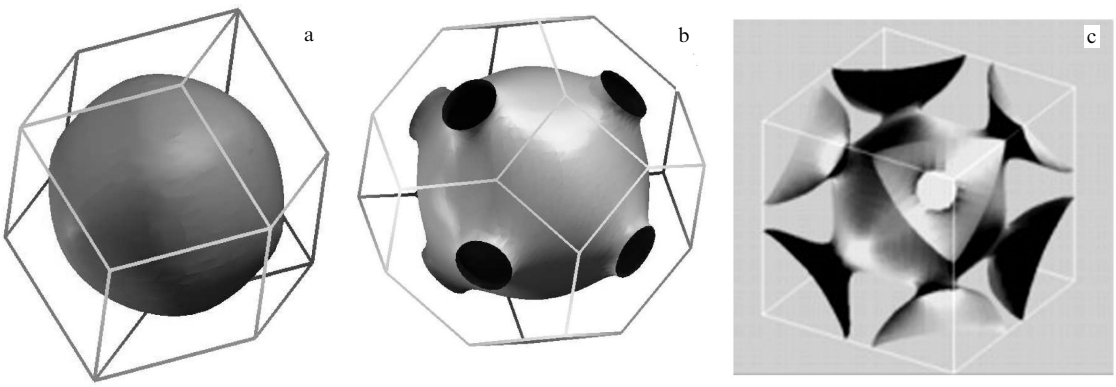

Figure 8. The Fermi surface of lithium with the bcc structure at normal pressure (a), and with the fcc structure at $P \sim 30$ GPa (according to Refs [66]) (b and c).

For lithium, after fcc, within a small pressure range (39–42 GPa) there exists an additional phase, a rhombohedrally distorted fcc phase. There are also data on new complex phases of Li and Na at still higher pressures [16, 67, 68]. At present, the structure of these phases is unknown, but one possible tendency could be a further enhancement of Hume-Rothery effects, which could lead to the formation of more complex structures in which the Brillouin zone would have a larger number of planes near the Fermi level.

4.2 Heavy alkali metals

The heavy alkali metals K, Rb, and Cs open the long periods in the periodic table, which include transition elements. The electron d-shells, filled in transition metals, are located above the valence s-level for alkali metals. When the metal is compressed the energy levels broaden and they are displaced in relation to one another [69]. In accordance with this assumption, the d-level lowers in relation to the s-band, which results in a partial s – d transition, as shown in Fig. 9. Usually, the existence of complex phases emerging in heavy alkali metals under pressure is explained by the electron s – d transition. However, the large number of structural transformations under pressure (six phases have been established for Rb and Cs) and the variety of structural types lead to the need to take into consideration other factors accompanying the compression of heavy alkali metals, which are discussed below.

4.2.1 The Rb-III and Cs-III phases related to Li-*cI*16. Let us begin with the first transitions to complex phases in Rb and Cs that appear after the bcc – fcc transition has been completed. For a long time it was believed that the phase Cs-III, which forms within a narrow pressure range 4.2–4.3 GPa, has an fcc structure and that in Cs an isostructural fcc – fcc transition related to an electron transition occurs. Recently the Cs-III structure has been identified as orthorhombic (the space group is $C222_1$, 84 atoms per unit cell, and the Pearson symbol is *oC*84) [4]. Rb-III has the same space group, 52 atoms per cell, and the Pearson symbol *oC*52 [52].

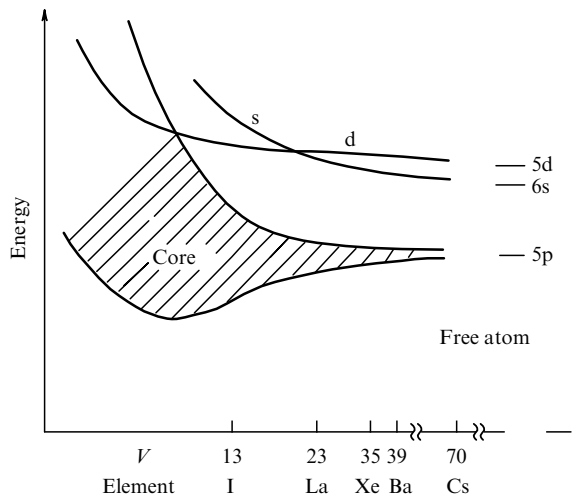

Figure 9. Schematic representation of the dependence of electron energy levels on the atomic volume V ($cm^3\ mol^{-1}$) for elements from iodine to cesium (according to Ref. [69]). When the metal is compressed, the 5d-level lowers in relation to the 6s-level, which results in an electron s–d transition. When the compression is extremely high, the levels of the valence band (5d–6s) and the inner electron orbitals (5p) may overlap.

Structurally, the Cs-*oC*84 and Rb-*oC*52 phases are related to the Li-*cI*16 phase and can be thought of as being distorted bcc-based superstructures [59, 60]. The cubic structure Li-*cI*16 can be represented by an orthorhombic cell with the axes $2 \times 2\sqrt{2} \times 2\sqrt{2}$ in relation to bcc. In the same way, Rb-*oC*52 can be represented by a superstructure with the axes $2 \times 2\sqrt{2} \times 3\sqrt{2}$ in relation to bcc and Cs-*oC*84 by a superstructure with the axes $2 \times 2\sqrt{2} \times 5\sqrt{2}$ in relation to bcc. If we examine Li-*cI*16, Rb-*oC*52, and Cs-*oC*84 from this angle, their common structure of blocks consisting of eight or ten atoms becomes obvious (Fig. 10a). The fact that there are two additional atoms (ten instead of eight) in some structural blocks for Rb and Cs may stem from the decrease in the overall number of valence electrons (s-type) per unit cell due to their transition to d-levels (an electron s–d transition). This is the reason for addition distortion of the structures Rb-III and Cs-III in comparison to Li-*cI*16. The common nature of these structures follows from the similarity of their diffraction patterns (Fig. 10b), with the difference primarily consisting in the splitting of the (211) reflection observed in Li-*cI*16 into a group of close reflections whose positions are near $2k_F$. The Brillouin zones built for Rb-III and Cs-III with planes corresponding to these reflections are shaped like the Brillouin zone for Li-*cI*16, as shown in Fig. 10c. This approach suggests that the Hume-Rothery mechanism is the main reason for the formation of the complex phases Rb-*oC*52 and Cs-*oC*84, just as it is for Li-*cI*16.

It is interesting to compare the formation of the complex phases Rb-III and Cs-III with variations in the resistivity of these metals [70]. In both cases, at 4.2 GPa for Cs-III and at 14 GPa for Rb-III, there is a sudden increase in electrical resistance (Fig. 11a). Here, we must note the structural similarity of the phases Rb-*oC*52 and Cs-*oC*84 with the phase Ga-*oC*104, which has the same space group $C222_1$ and a similar mechanism of complex supercell formation [52]. Earlier, we noted that in the transition to the phase Ga-*oC*104 the resistance suddenly increases in comparison to that of the Ga-fct phase [56], and the assumption is that in the process of formation of phases of the Hume-Rothery type there is a drop in the density of electron states at the Fermi level and a reduction in the area of the Fermi surface, which leads to a decrease in the number of electrons participating in conduction. We mentioned earlier the increase in electrical resistance caused by the enhancement of Hume-Rothery effects for the case of gamma brass.

4.2.2 The structures *tI*4 and *oC*16 for Rb and Cs. After rubidium and cesium under pressure have reached the structurally related phases *oC*52 and *oC*84, phases with the structure *tI*4 are formed under greater compression [71, 72]. For rubidium, between the phases Rb-III (*oC*52) and Rb-V (*tI*4) in the pressure range from 17 to 20 GPa there appears another phase Rb-IV with a host – guest structure [10], which we discuss below together with similar structures in alkali-earth metals.

A characteristic feature of the formation of the phase *tI*4 in Rb and Cs is the drop in electrical resistance, as shown in Fig. 11a, in contrast to an increase in resistance for the *oC*52 and *oC*84 phases. This suggests the electron state in these phases are different.

The tetragonal phase *tI*4 has a space group $I4_1/amd$, just as β-Sn does, but a different ratio $c/a = 3.73$ (instead of ~ 0.54 for β-Sn). The coordination number for the *tI*4 phase is $4 + 4$, which is a smaller than the coordination number in

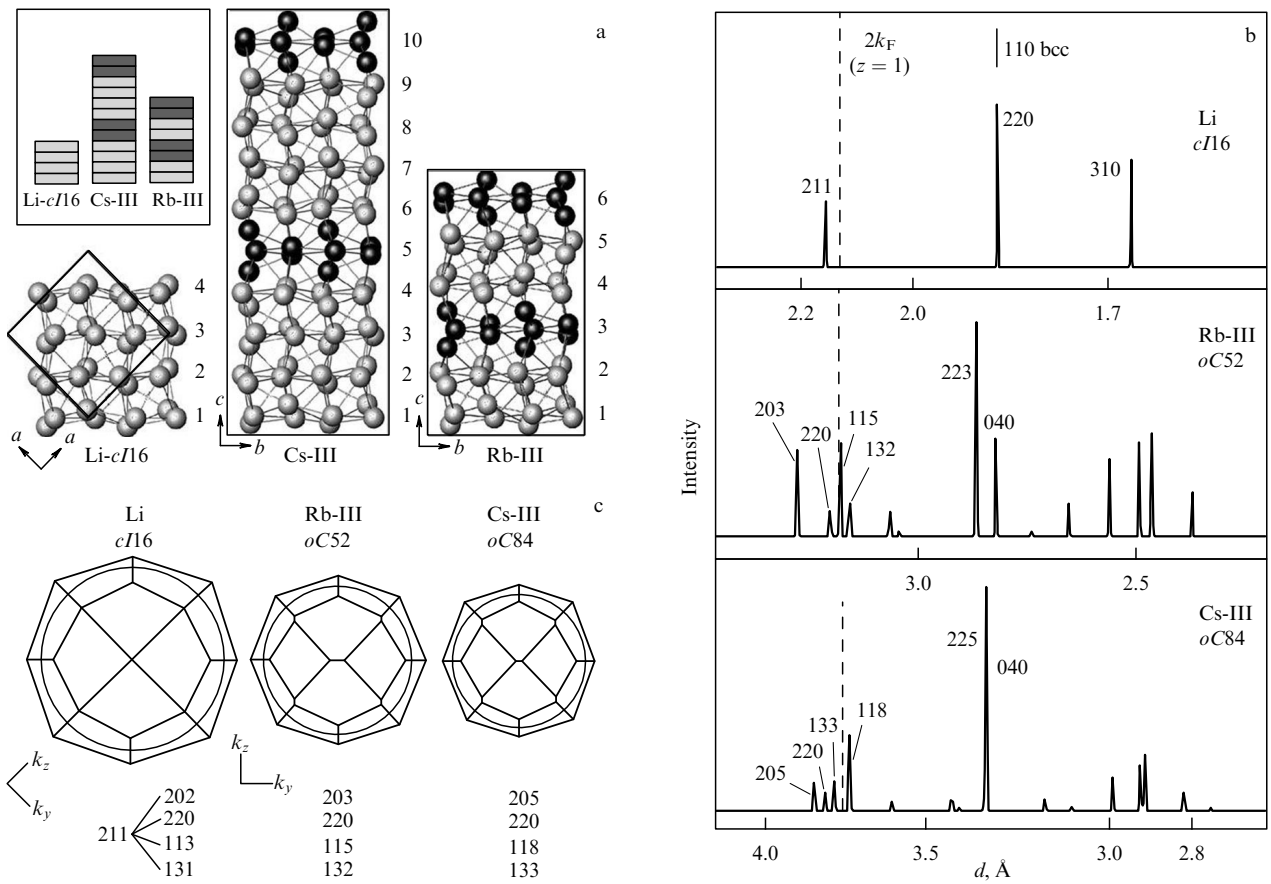

Figure 10. The structures Li-*cI*16, Cs-*oC*84, and Rb-*oC*52. (a) Representation of the structures by superstructures in relation to bcc. The inset shows the packings of identical layers of eight atoms (gray) and ten atoms (black). (b) Diffraction patterns of the phases (the values of the interplanar spacing d are shown on the logarithmic scale); the position of $2k_F$ is shown for $z = 1$. (c) The Brillouin zones with planes corresponding to the structural reflections near $2k_F$ (from Refs [59, 60]).

the fcc structure (12) and smaller than the coordination number in the *oC*52 and *oC*84 phases (10 – 11). With this reduction in the value of the coordination number, the packing density of the structure, η (the ratio of the volume occupied by the atoms to the cell volume), decreases, which is possible only if the atomic radius decreases considerably in the structural transformation. One must also allow for the change in the atomic volume as a result of the transformation; for cesium $\Delta V(\mathrm{II}-\mathrm{III}) = 6.4\%$ and $\Delta V(\mathrm{III}-\mathrm{IV}) = 6.1\%$ [4]. Assuming that for *tI*4 the packing density $\eta = 0.56$ (when the atomic radius is estimated from the shortest distance in the structure, equal to the period a) and fixing $\Delta V(\mathrm{II}-\mathrm{IV})$ at 12%, we can estimate the variation in the atomic radius R in the *tI*4 structure in comparison to fcc ($\eta = 0.74$):

$$\frac{R_{\mathrm{fcc}}}{R_{tI4}} = \left(\frac{\eta_{\mathrm{fcc}}}{0.88\eta_{tI4}}\right)^{1/3} = 1.14\,.$$

This corresponds to a decrease in the atomic radius for Cs in II – III – IV transitions by $\sim 14\%$. A slight decrease in the atomic radius in the II – III transition should be attributed to an s – d transition, but the transition into the *tI*4 phase with a substantial decrease in R, the packing density, and the coordination number requires a different mechanism, which we consider below.

The next phase for Cs and Rb in the chain of transformations under pressure is also a common phase with the structure *oC*16-*Cmca* [1, 73]. This type of structure was first found in Cs-V. What was remarkable was the discovery of a similar structure in the group IV elements Si and Ge [2, 74]. The assumption that such a structure can exist in the binary alloys Bi – In and Bi – Pb also made it possible to decipher the diffraction data on high-pressure phases in these alloys [75]. In the equiatomic alloy BiSn, a phase with the structure *oC*16-*Cmca* was produced under pressure; it was found that in it the Bi and Sn atoms are arranged in an orderly way in the positions 8d and 8f, respectively [76]. A solution based on the structure *oC*16-*Cmca* was also found for the phase Bi-IV (3.9 GPa, 503 K) [75].

Thus, the *oC*16 structure is a characteristic feature of the high-pressure phases of polyvalent metals, group IV and V elements, and Bi-based alloys. The use of the Fermi sphere – Brillouin zone interaction concept and construction of the Brillouin zone for strong reflections near $2k_F$ indicate that this structure is stabilized by the Hume-Rothery mechanism (Fig. 12). What is important is that the Brillouin zone constructed for the first strong diffraction peaks is shaped like a symmetric polyhedron with almost perfect hexagonal cross sections in several directions. This fact is significant for the minimization of the electrostatic contribution and is reflected in the special value of the ratios $b \approx c \approx a/\sqrt{3}$ for all the phases with structure *oC*16-*Cmca* discovered so far.

The formation in the alkali metals Cs and Rb of phases with the structure *oC*16, which is a typical structure for polyvalent metals, may lead to the question of how many free electrons exist in the conduction band in these phases of alkali metals or, in other words, of the possibility of the

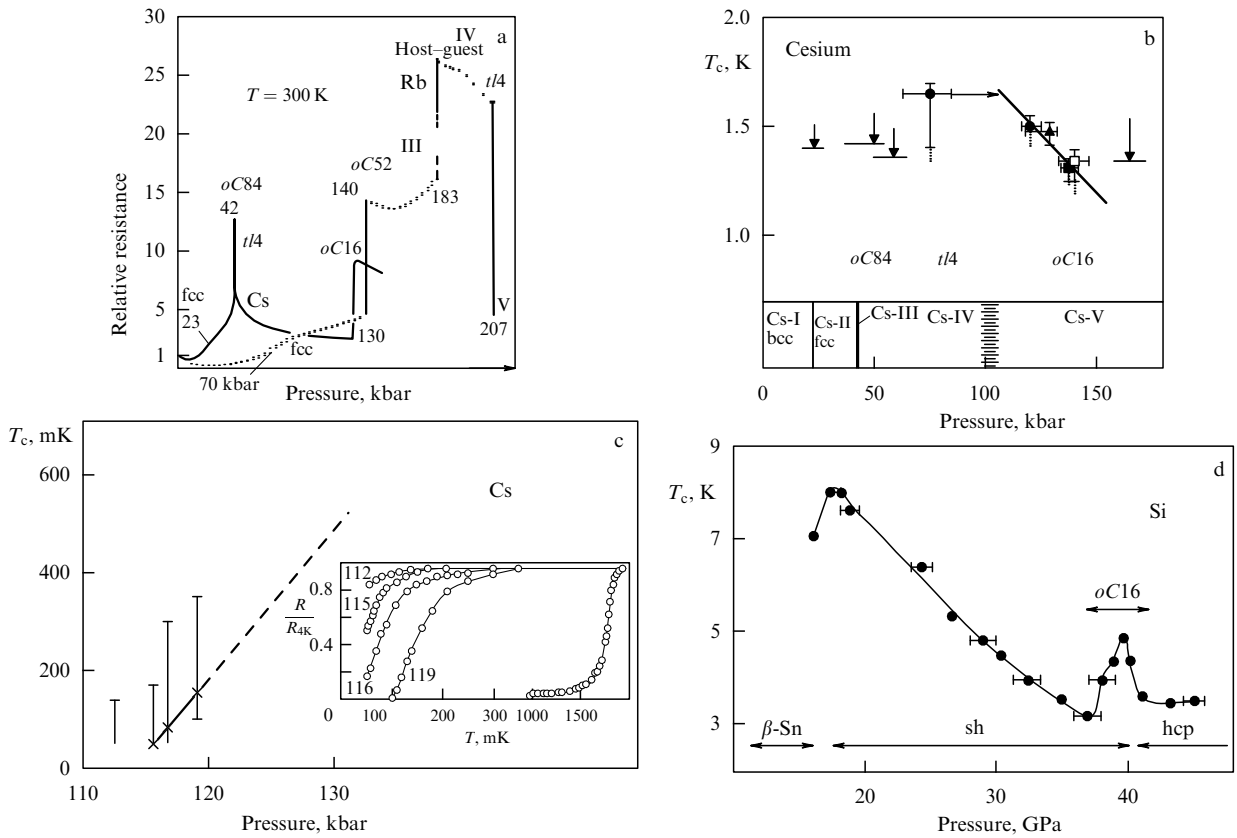

Figure 11. (a) Electrical resistance of Rb and Cs under high pressure (from Ref. [70]), with the numbers indicating pressure measured in kbar; shown are an increase in resistance as the transitions to complex phases Cs-$oC84$ and Rb-$oC52$ and the transition to Rb-IV (host–guest phase) take place and a decrease in the resistance of Cs and Rb as the transition to the $tI4$ phase takes place. (b) Superconductivity of Cs at 12–14 GPa: $T_c = 1.3-1.5$ K for the Cs-V $oC16$ phase, upon reduction in pressure the phase is retained with $T_c = 1.65$ K at 7.5 GPa (from Ref. [77]). (c) Superconductivity of Cs with $T_c = 0.1-0.3$ K in the Cs-IV $tI4$-phase at 11–12 GPa; the pressure values indicated in the inset are in kbar (from Ref. [78]). (d) The pressure dependence of T_c for silicon (from Ref. [79]); after the minimum $T_c = 3.3$ K at 37 GPa there is an increase in the superconductivity transition temperature to 4.9 K at 40 GPa in the $oC16$ phase followed by a drop in the hcp phase.

valence band overlap the electron levels of the core. Volume compression of Rb and Cs in the transition to these phases amounts to 0.2 and 0.25, respectively. One can assume that already in the $tI4$ phase, due to the reduction in the packing density in this structure and the decrease in the atomic radius, there begins the above-mentioned overlap of the valence band and the core levels. With such an assumption, the drop in electrical resistance in the $tI4$ phase for Cs and Rb may be connected to the increase in the number of electrons in the conduction band due to the influx of electrons from the inner orbitals of the core. The possibility of hybridization of sp- and d-orbitals as the volume gets smaller because of the lowering of d-levels and the rising of inner p-levels has been examined by Ross and McMahan [69] (see Fig. 9). According to theoretical calculations, such overlap of core electron levels and the valence band occurs at much greater compression.

Finalizing the discussion of heavy alkali metals, we should mention the discovery of superconductivity in Cs under pressure [77, 78]. Cesium becomes superconducting in the $tI4$ phase with $T_c = 0.1-0.3$ K at 11 – 12 GPa. The sudden jump in T_c to 1.3 K at 13 – 14 GPa corresponds to a transition to the $oC16$ phase, while decreasing the pressure leads to $T_c = 1.65$ K at 7.5 GPa (Fig. 11b). For the sake of comparison, we note the substantial increase in T_c for Si as the pressure rises within the stability range of the $oC16$ phase [79] (Fig. 11d). A high value of T_c is a characteristic feature of the $oC16$ phase in bismuth alloys. The value of T_c obtained for the BiSn alloy is 7.4 K at 3 GPa after annealing at 363 K [80]. The intermediate high-pressure phases of Bi – In and Bi – Pb alloys, whose structure has recently been identified as $oC16$ [75], also exhibit high values of T_c, from 7.5 to 8.7 K [81, 82]. For Cs and Si we note the relation that exists between the rise in T_c and the enhancement of the Hume-Rothery effects in the $oC16$ phase.

Note that we have not discussed pressure-induced transformations in potassium, for which transitions bcc – fcc – complex phase of the host – guest type have been discovered. Here, the last phase is similar to Rb-IV [16], which is considered below together with similar phases in alkali-earth metals.

5. Alkali-earth metals at high pressure

The lighter alkali-earth metals Ca and Sr have at normal pressure an fcc structure and transform into bcc under compression, while the heavier alkali-earth metal Ba already has a bcc structure at normal pressure. Usually the fcc – bcc transformation is related to an s – d transition, which progresses as we move from one element of the group to another and occurs for heavier alkali-earth metals at lower pressures; for Ba this transition occurs already at atmospheric pressure.

The next transition for Ca and Sr happens when these elements are compressed to 0.43 – 0.44 of the initial volume V_0

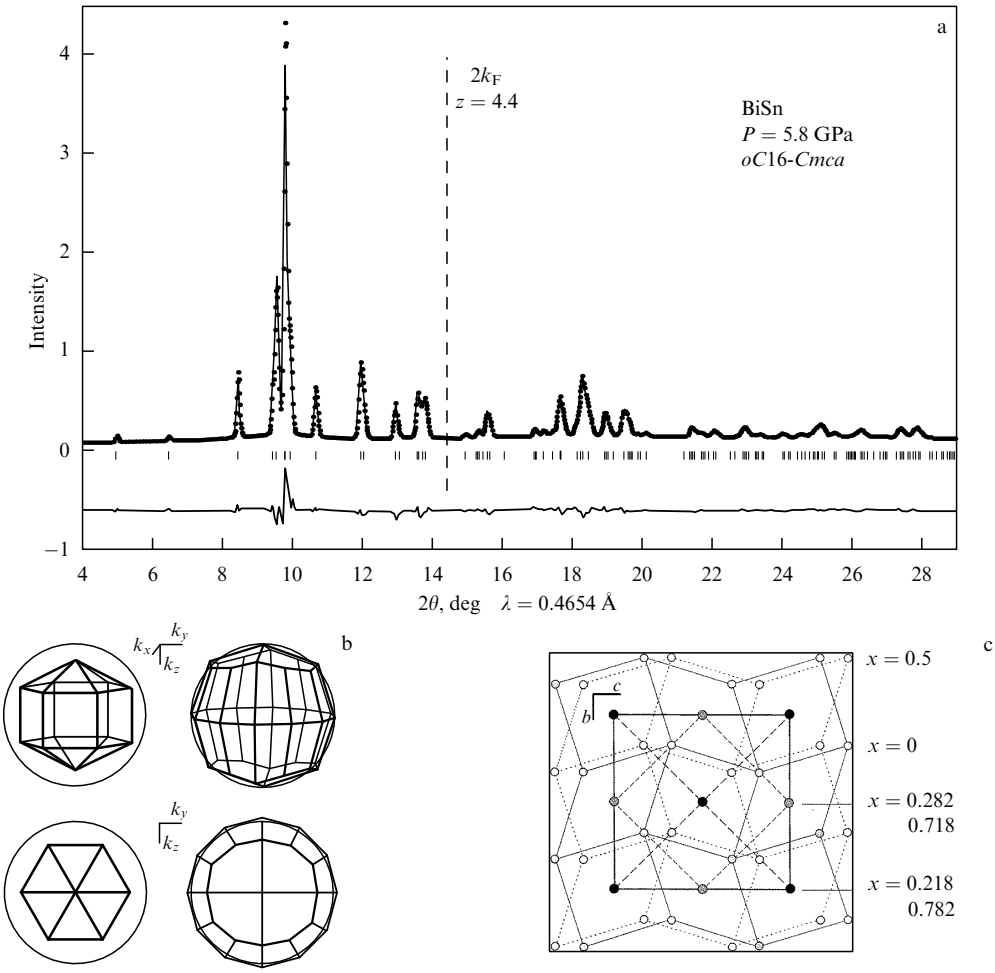

Figure 12. The structure $oC16$-$Cmca$ in the BiSn alloy (from Ref. 76). (a) Diffraction pattern of the phase $oC16$ of BiSn at 5.8 GPa; the vertical dashed line indicates the position of $2k_F$ for $z = 4.4$. (b) Brillouin zones: to the right, for planes corresponding to the first strong structural reflections, (112), (202), (220), and (400); to the left, for the planes (113), (131), (421), and (511) located near $2k_F$; the volume of the Brillouin zone accommodates 4.3 electron states. (c) The locations of the atoms in the $oC16$ structure; depicted is the projection along [100]; atoms in the 8f position for $x = 0$ and 0.5 form nets 3^2434, and atoms in the 8d position form square nets for x and $1/2 - x$ ($x = 0.218$). For the phase of BiSn there is an ordered arrangement of Sn atoms in the 8f positions and Bi atoms in the 8d positions.

into structures with a reduced packing density and coordination number. Calcium transforms at $P = 32$ GPa into a simple cubic (sc) structure with a coordination number of six [83]. This phase is stable within a broad pressure range extending to 113 GPa and transforms into a complex structure, which has yet to be solved [84].

For Sr, the next phase after bcc has the β-Sn structure in a pressure range extending from 26 to 35 GPa and at $P = 35$–49 GPa Sr has a complex monoclinic phase $mI12$, which can be considered a superstructure in relation to the cell of β-Sn with a triple cell volume [85, 86]. At above 50 GPa, there emerges the phase Sr-V with a host – guest structure stable up to high pressures (< 117 GPa) [7]. The phase Ba-IV has the same structure in a pressure range extending from 12 to 45 GPa [6]. Below we analyze in detail the recently established structures of the alkali-earth metal phases and compare them with the electrophysical properties of these phases.

5.1 The simple cubic structure in calcium and the β-Sn phase in strontium

The packing density of the sc structure amounts to 0.52 and is lower than 0.62 for bcc. The bcc – sc transition results in a substantial decrease in the atomic radius R calculated on the assumption that the atoms in the structure are in contact. Allowing for the jump in volume $\Delta V(\text{bcc}-\text{sc}) = -8\%$ at 32 GPa, we can estimate the ratio of the atomic radius for Ca in these structures:

$$\frac{R_{\text{bcc}}}{R_{\text{sc}}} = \left(\frac{\eta_{\text{bcc}}}{0.92\eta_{\text{sc}}}\right)^{1/3} = 1.12\,.$$

A decrease in the Ca radius by 12% in the bcc – sc transition corresponds, in magnitude, to the decrease in the Cs radius in the fcc – $tI4$ transition, as explained earlier.

The sc structure is realized under pressure in group V elements phosphorus and arsenic. The sc structure in phosphorus exists at 10 – 110 GPa, and in this structure phosphorus is a superconductor with $T_c = 9.5$ K at 35 GPa [87]. The sc structure in arsenic is stable in the pressure range extending from 25 to 48 GPa and exhibits superconducting properties with T_c up to 2.5 K [88]. Calcium also becomes a superconductor in the sc phase with $T_c = \sim 5-7$ K (Fig. 13). The superconductivity transition temperature of calcium grows to 15 K at 150 GPa [89], but such high values of T_c for Ca are attained in a phase with a complex structure, which has yet to be determined.

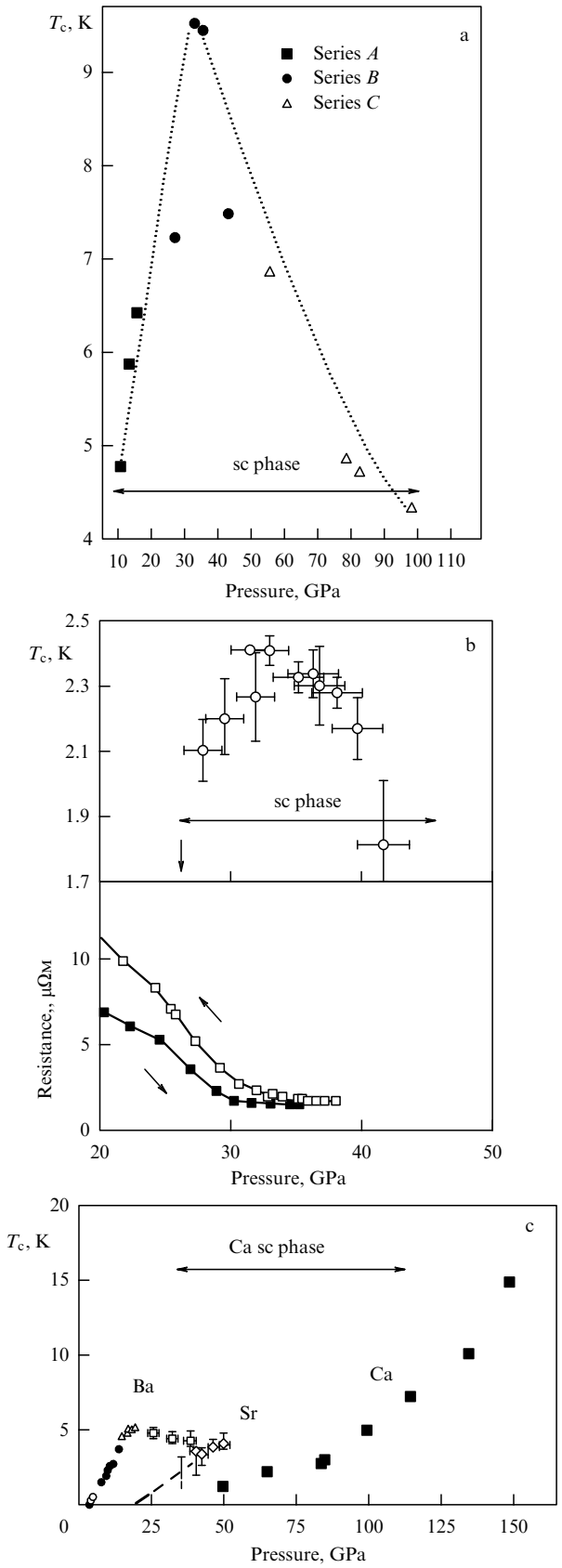

Figure 13. Superconductivity of elements in phases with a simple cubic (sc) structure (from Refs [87–89]): (a) phosphorus, (b) arsenic, and (c) calcium (compared to Ba and Sr).

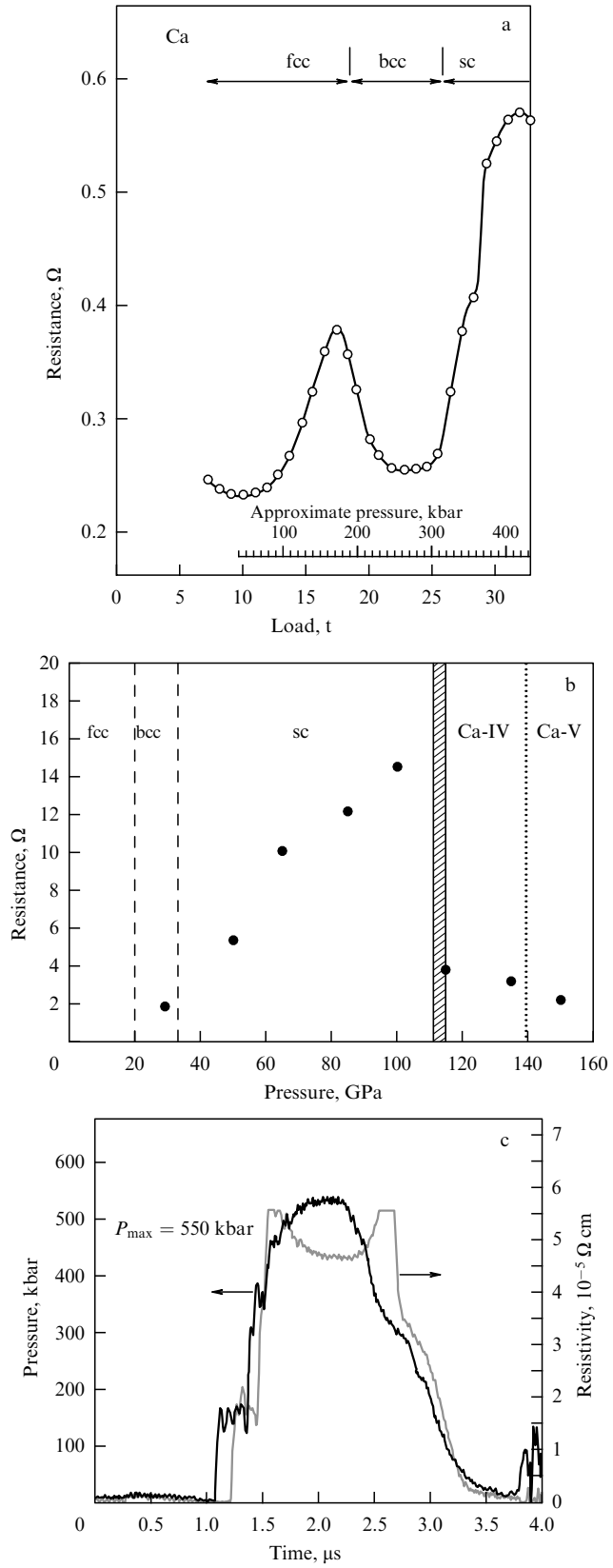

Figure 14. Electrical resistance of Ca at high pressure: (a and b) static loading (from Ref. [90]), and (c) dynamic loading (from Ref. [91]).

Using the Fermi sphere – Brillouin zone interaction model for the sc-Ca phase shows that this structure is not favored energetically at $z = 2$. We could attempt to explain the stability of the sc-Ca within this model based on the

assumption that z takes on values between three and four. For such a value of z, due to Hume-Rothery effects, there could be an increase in electrical resistance of Ca like the one observed experimentally at static compression [90] and at shock-wave compression [91] (Fig. 14). This possibility can be discussed, as in the case of alkali metals, only if we take into account the overlap of the valence band and the core electron states. However, for Ca, as for Cs, it has been shown via theoretical research that the overlap of valence and inner electron orbitals emerges at much greater compressions and that the features of the structure and electrophysical properties of Ca under pressure, including the above-mentioned increase in electrical resistance as well as the subsequent decrease [91] (Fig. 14b), can be explained by the overlap of the outer electron levels of the s – d or sp – d type (e.g., see Refs [69, 18]).

Superconductivity in Sr emerges in the β-Sn phase and increases in the next phase, a distorted β-Sn phase, to 4 K [92]. Even higher values of T_c (up to 7 K) have been attained in the Sr-V host – guest phase, which we will now discuss.

5.2 The host – guest phase in heavy alkali-earth metals

The discovery of an incommensurate (host – guest) phase in Ba-IV was quite unpredictable. The announcement about the first incommensurate phase in an element was made at the Eighteenth International Congress of Crystallography held in Glasgow in 1999 by a group of researchers from Edinburgh headed by R J Nelmes [6]. A similar phase was also found for Sr-V [7]. Such discoveries were made possible by the development of methods for studying single crystals at high pressure. In the process of discussing these results, the present author suggested that such a structure may exist in the Bi-III phase, for which earlier a monoclinic structure had been proposed, but the atom arrangement was found to be similar to that in the host – guest structure of Ba-IV. Indeed, as a result of single-crystal studies of Bi-III an incommensurate structure close to that of Ba-IV but with a difference for the guest structure was established [8]. In accordance with the homology rule, such an incommensurate structure also forms in other group V elements, Sb and As [8, 9].

The host – guest crystal structure for Bi-III (Fig. 15) consists of square-triangular nets in the *ab* plane that are packed along the *c* direction in such a way that the squares in the neighboring layers are aligned but their sides are turned, so that they form channels along the *c*-axis, in which the chains of the guest atoms are located. The distances between the atoms in the chains are incommensurate with the period *c* of the tetragonal host substructure, and the guest substructure formed by the chains can be characterized by a tetragonal cell whose periods *a* and *b* are the same as in the host substructure but the period *c* is different. The periods *c* of the two substructures are incommensurate: their host-to-guest ratio is ~ 1.31 for Bi-III. The chains of guest atoms form sublattices of different types in different elements, e.g., a body-centered tetragonal sublattice for Bi and Sb and a base-centered tetragonal one for Ba and Sr. Guest chains can rearrange for an element within the limits of existence of a particular host – guest phase, e.g., transforming from a tetragonal cell to a monoclinic cell (Sb and Ba), forming superstructures and even 'melting', i.e., losing the mutual correlation and long-range order in their arrangement, as is the case for Rb-IV [11]. This points to a special type of coupling in the guest chains, which, possibly, is of a localized d-nature.

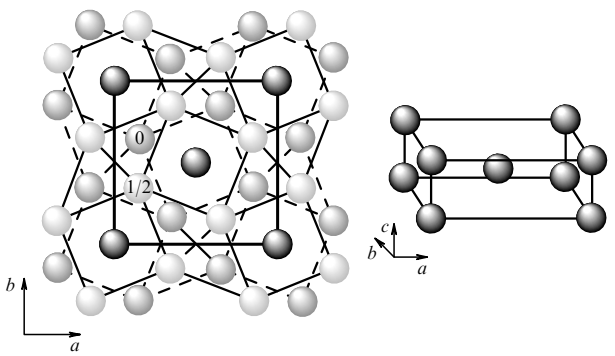

Figure 15. The host–guest structure for Bi-III (according to the data of Ref. [8]). To the left, nets of 3^2434 host atoms at the levels $z = 0$ (dark gray spheres) and $z = 1/2$ (light gray spheres) are shown by solid and dashed lines, respectively. Guest atoms are depicted as black spheres. To the right, a general view of the guest sublattice with a tetragonal body-centered cell is shown to the same scale.

The formation of high-pressure phases of similar structure for alkali-earth metals and group V elements suggests that the elements in these phases have similar valence-electron structures, whose characteristic feature is the presence of d-bonding in the atomic chains. The electrophysical properties of these phases also behave similarly. First, we note the characteristic jump-like increase in resistance in the course of the II – III transition for Bi and an almost equal drop in the course of the III – V transition from host – guest to bcc [93] (Fig. 16a). Barium exhibits a similar increase in resistance in the course of the transition from hcp to host – guest (Fig. 16b). Such a rise in resistance in the incommensurate phase can be attributed to chain formation involving the d-bonds, which leads to a decrease in the number of free electrons participating in conduction.

The incommensurate phase in the alkali metal Rb at 17 – 20 GPa also exhibits chains in the guest substructure, although the host substructure has another atomic configuration [10] than that of Ba, Sr, and group V elements. The increase in resistance in the course of the transition from Rb-III to Rb-IV should be attributed solely to the chain formation involving the d-bonds (Fig. 11a).

The formation of the incommensurate phases in Sb, Bi, Ba, and Sr shows correlation with relatively high values of T_c (for Bi-III $T_c = 7.2$ K at 2.8 GPa [94], for Sb-II $T_c = 3.55$ K at 8.5 GPa [95], for Ba-IV $T_c = 5$ K at 14 GPa [96], and for Sr-V $T_c = 7$ K at 45 GPa [92]) (Figs 16c and 16d).

6. Conclusion

The above discussion of structural transformations under pressure for certain elements and the comparison of these transformations with changes in the electrophysical properties give a general picture of the manifestation of the different factors that determine the structure and properties of simple metals under compression. It is interesting to follow the changes in the superconducting properties of Ba in connection with its structural transformations bcc – (5.5)hcp – (12)host – guest – (45)hcp (the numbers in parentheses represent the respective pressures in GPa). Superconductivity emerges already in the bcc phase ($T_c = 0.06$ at 3.7 GPa) and increases within this phase (0.5 K at 4.8 GPa) [97]. For the hcp phase $T_c = 1.3$ K at 5.5 GPa, and T_c grows with pressure to roughly 2.7 K. The formation of the host – guest phase is related to a substantial increase in T_c to 5 K at 14 GPa [96]. As

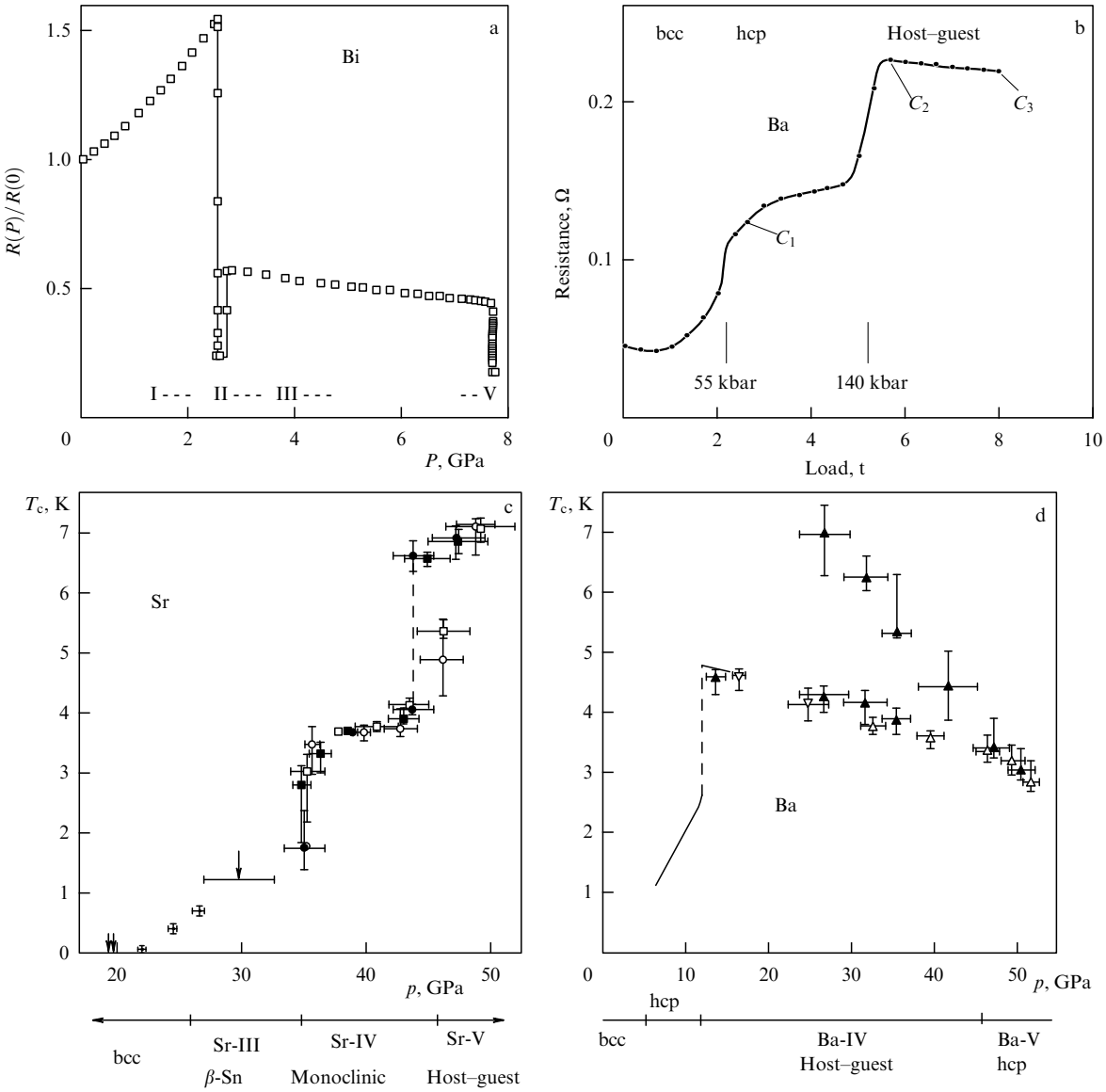

Figure 16. (a and b) Pressure dependence of electrical resistance for Bi (from Ref. [93]) (a) and for Ba (from Ref. [96]) (b). The superconducting transition temperature for Ba at point C_1 is about 2 K and at point C_2, 5 K. (c and d) Superconductivity of Sr (c) and Ba (d) under pressure (from Ref. [92]). The host–guest phase has a transition temperature T_c equal to 7 and 5 K for Sr and Ba, respectively. For the Ba-V hcp phase the transition temperature $T_c = 7$ K is observed on decompression.

the pressure grows, T_c in this phase slowly drops and T_c equal to 4 K observed at 46 GPa in the next phase of Ba-V (hcp). The last phase retains its stability as the pressure is decreased to 25 GPa, with T_c increasing to 7 K (Fig. 16d).

An analysis of the pressure dependence of T_c leads to the following conclusions concerning the changes in the electronic properties of Ba in the various phases. We can assume that in the bcc phase superconductivity emerges and T_c rises due to enhancement of Hume-Rothery effects under pressure, as is the case with fcc lithium. The higher values of T_c in the hcp phase should be attributed to the s – d transition and also the enhancement of Hume-Rothery effects. The rapid increase in T_c in a transition to the host – guest structure is, probably, related to the subsequent overlap of the electron levels (the compression at 12.8 GPa amounts to 0.48) and the strengthening of the d-bonding. The lowering of T_c with increasing pressure is typical for normal metals. The different behavior of T_c for the two phases of Ba with the same hcp structure indicates that the electronic structures of these phases are very different. The high values of T_c for Ca indicate that the complex phase of Ca that forms after the sc phase may be of the host – guest type [84]. For this phase, in accordance with the earlier discussion, we can expect the valence band to overlap core electron levels and the d-bonding to become stronger.

Thus, the nature of variations in the electrophysical properties of metals under pressure correlates with the crystal structure and the valence electron state of the new phases. The increase in resistance is associated with the enhancement of Hume-Rothery effects, i.e., an increase in the density of states below the Fermi level and a decrease in the density of states directly at the Fermi level (a reduction in the free Fermi surface). Another effect that leads to an increase in electrical resistance is a decrease in the number of free charge carriers due to d-bonds formation (a chain bonding), i.e., caused by s – d or sp – d transitions (in group

V elements). This is the cause of a rise in the density of states near the Fermi level and results in fairly high values of T_c for phases with a host – guest structure.

By systematizing and analyzing the data on the structure and properties of alkali and alkali-earth metals and group IV and V elements we can arrive at the following conclusions.

1. The transition of alkali metals under pressure from bcc to fcc and then to the complex phases Li-*cI*16, Rb-*oC*52, and Cs-*oC*84 is related to the Hume-Rothery mechanism, the formation of planes of the Brillouin zone near the Fermi surface, which lowers the energy of the electrons and, correspondingly, the energy of the crystal structure.

2. The relative complexity of the phases Rb-*oC*52 and Cs-*oC*84, compared to Li-*cI*16, is caused by a partial s – d transition in heavy alkali metals.

3. The formation of phases with a host – guest structure in alkali and alkali-earth metals under considerable compression should be attributed to the strengthening and localization of d-bonds accompanied by the formation of atomic chains.

4. In group V elements the valence electrons of sp-levels and a higher d-level which decreases as the pressure grows may hybridize, which leads to the formation of chain incommensurate structures similar to the structures of alkali-earth metals.

The formation of hybrid spd-bonds under compression constitutes a general phenomenon for polyvalent elements and manifests itself under pressure in group VI and VII elements. This has been recently demonstrated by the discovery of a new type of structures, incommensurately modulated structures, in the group VII element iodine [12] and in group VI elements tellurium, selenium, and sulfur [13, 14]. The discovered phases emerge at the metallization threshold of these elements. Modulated structures of group VI elements consist of atomic chains with minimum interatomic distance that are packed parallel to each other with a relative shift in the arrangement of the chains such that the atoms in neighboring chains form a modulation wave incommensurate with the cell period *b*, as shown in Fig. 17. The nature of the atomic bonds in the chains of incommensurate phases of different group V and VI elements with d-electron participation can be assumed to be the same. Roughly a quarter of all atoms participate in chain formation in group V elements, while all atoms participate in chain formation in group VI elements, which indicates a larger number of electrons participating in the d-bonds. This assumption agrees with the discovery of superconductivity in the modulated phases for iodine and group VI elements with fairly high values of T_c (1.2 K for iodine, 4.2 K for tellurium, 5.8 for selenium, and 10 – 14 K for sulfur). The superconducting properties of these elements under pressure are discussed in Refs [14, 98].

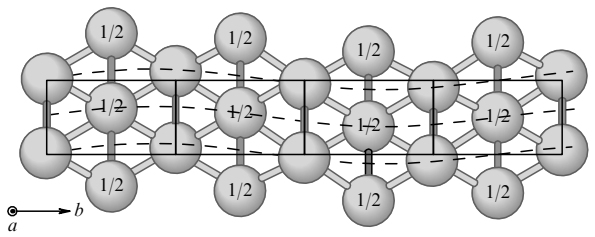

Figure 17. The incommensurately modulated structure Te-III stable in the pressure range from 4.5 to 29 GPa (from Ref. [13]). The unit cell is body-centered monoclinic with the following parameters: $a = 3.918$ Å, $b = 4.733$ Å, $c = 3.061$ Å, and $\beta = 113.5°$, at 8.5 GPa. Shown are four cells in the projection along the *a*-axis. The atoms centering the cells are labeled '1/2'. Interatomic distances with fixed values are depicted dark, and interatomic spacing with variable, or modulated, values are depicted light. The distances along the *c*-axis are constant, i.e., the atoms form rigid chains with relative displacements along the *b*-axis. The modulation wave is depicted by dashed curves. The modulation vector (0, *q*, 0) has a length $q = 0.28$ and is incommensurate with the period *b*. Similar structures have been detected in other group VI elements, such as selenium (at 28 – 80 GPa) and sulfur (at 83 – 153 GPa) (from Refs [13, 14]).

The history of the discovery of new structures in elements under pressure is far from finished. The elements in the left and right parts of the periodic table separated by transition metals exhibit remarkable similarity. One more example of complex behavior under pressure is scandium, which is at the beginning of the transition-metal series. Its structure under normal pressure is hcp. Five new phases have been discovered in Sc in a pressure range extending to 297 GPa [99], and the structure of these phases is being studied. We can expect the formation of structures of the host – guest type with localized d-bonds, as well as structures with lower packing densities similar to the phases of alkali and alkali-earth metals. A hint of this is given by the recent report concerning the detection of an incommensurate host – guest structure for Sc-II at pressures higher than 20 GPa [100], corresponding to the earlier discovered jump-like increase in resistance and superconductivity in this phase ($T_c = 0.35$ K at 21 GPa) [101].

The main factors influencing the structure of simple sp-metals discussed in this review are related to the two main contributions to the energy of the crystal state, the electrostatic and the valence electron band contributions. The balance between these contributions when such metals are compressed is shifted with the electron contribution becoming larger, which strengthens the interaction between the Fermi surface (close to a sphere for simple metals) and the planes of the Brillouin zone. The Fermi sphere – Brillouin zone interaction is the decisive factor for the structure of some simple metals and alloys, e.g., Hume-Rothery phases in Cu – Zn alloys and tetragonal phases in indium and tin alloys. The structure of the phases in these systems is determined by the electron concentration and the stability of the phases is determined by the interplay between the Fermi sphere and the Brillouin zone, or by the Hume-Rothery effects. Experimental studies have shown that applying pressure to these alloys enhances the Hume-Rothery effects. The complex behavior of simple metals (alkalis and alkali earths) under high pressure, consisting in the transition from typically metallic, compact, and high-symmetry structures (fcc, bcc, and hcp) to structures with reduced packing density and coordination number, is the manifestation of changes in the electron subsystem and is accompanied by a nonmonotonic behavior of electrophysical properties. Structural transformations under high pressure with a tendency for reducing the symmetry and packing density are related to the enhancement of the Hume-Rothery effects, i.e., the interaction between the Fermi sphere and the Brillouin zone.

The author is grateful to E G Ponyatovskii, V E Fortov, and E G Maksimov for the fruitful discussions. This work was made possible by support from the Russian Foundation for Basic Research (Grant No. 04-02-17343).

References

1. Schwarz U et al. *Phys. Rev. Lett.* **81** 2711 (1998)
2. Hanfland M et al. *Phys. Rev. Lett.* **82** 1197 (1999)

3. Hanfland M et al. *Nature* **408** 174 (2000)
4. McMahon M I, Nelmes R J, Rekhi S *Phys. Rev. Lett.* **87** 255502 (2001)
5. Nelmes R J et al. *Phys. Rev. Lett.* **88** 155503 (2002)
6. Nelmes R J et al. *Phys. Rev. Lett.* **83** 4081 (1999)
7. McMahon M I et al. *Phys. Rev. B* **61** 3135 (2000)
8. McMahon M I, Degtyareva O, Nelmes R J *Phys. Rev. Lett.* **85** 4896 (2000)
9. Degtyareva O, McMahon M I, Nelmes R J *High Press. Res.* **24** 319 (2004)
10. McMahon M I, Rekhi S, Nelmes R J *Phys. Rev. Lett.* **87** 055501 (2001)
11. McMahon M I, Nelmes R J *Phys. Rev. Lett.* **93** 055501 (2004)
12. Takemura K et al. *Nature* **423** 971 (2003)
13. Hejny C, McMahon M I *Phys. Rev. Lett.* **91** 215502 (2003)
14. Degtyareva O et al. *Phys. Rev. B* **71** 214104 (2005)
15. Kolobyanina T N *Usp. Fiz. Nauk* **172** 1361 (2002) [*Phys. Usp.* **45** 1203 (2002)]
16. Syassen K, "Simple metals at high pressure", in *High Pressure Phenomena, Varenna, Italy, July 3–13, 2001* (Proc. of the Intern. School of Physics "Enrico Fermi", Course 147, Eds R J Hemley et al.) (Amsterdam: IOS Press, 2002) p. 251
17. Schwarz U *Z. Kristallogr.* **219** 376 (2004)
18. Maksimov E G, Magnitskaya M V, Fortov V E *Usp. Fiz. Nauk* **175** 793 (2005) [*Phys. Usp.* **48** 761 (2005)]
19. Ashcroft N W, Mermin N D *Solid State Physics* (New York: Holt, Rinehart and Winston, 1976) [Translated into Russian (Moscow: Mir, 1979)]
20. Kittel Ch. *Introduction to Solid State Physics* (New York: Wiley, 1976) [Translated into Russian (Moscow: Nauka, 1978)]
21. Harrison W A *Pseudopotentials in the Theory of Metals* (New York: W.A. Benjamin, 1966) [Translated into Russian (Moscow: Mir, 1968)]
22. Heine V 'The pseudopotential concept', Cohen M L, Heine V 'The fitting of pseudopotentials to experimental data and their subsequent applications', Heine V, Weaire D 'Pseudopotential theory of cohesion and structure', in *Solid State Physics: Advances and Applications* (Eds H Ehrenreich, F Seitz, D Turnbull) Vol. 24 (New York: Academic Press, 1970) p. 1, 38, 250 [Translated into Russian, in *Teoriya Psevdopotentsiala* (Pseudopotential Theory) (Moscow: Mir, 1973)]
23. Hume-Rothery W *J. Inst. Met.* **35** 319 (1926)
24. Mott N F, Jones H *The Theory of the Properties of Metals and Alloys* (Oxford: The Clarendon Press, 1936)
25. Pearson W B *A Handbook of Lattice Spacings and Structures of Metals* Vol. 2 (New York: Pergamon Press, 1967)
26. Degtyareva V F et al. *J. Phys.: Condens. Matter* **17** 7955 (2005)
27. Mountfield K R, Rayne J A *Phys. Rev. B* **27** 3263 (1983)
28. Bain E C *Trans. AIME* **70** 25 (1924)
29. Donohue J *The Structure of the Elements* (New York: Wiley, 1974)
30. Young D A *Phase Diagrams of the Elements* (Berkeley: Univ. of California Press, 1991)
31. Alippi P, Marcus P M, Scheffler M *Phys. Rev. Lett.* **78** 3892 (1997); Marcus P M, Alippi P *Phys. Rev. B* **57** 1971 (1998)
32. Vereshchagin L F, Kabalkina S S, Troitskaya Z V *Dokl. Akad. Nauk SSSR* **158** 1061 (1964) [*Sov. Phys. Dokl.* **9** 894 (1965)]
33. Takemura K *Phys. Rev. B* **44** 545 (1991); Takemura K, Fujihisa H *Phys. Rev. B* **47** 8465 (1993)
34. Takemura K, Kobayashi K, Arai M *Phys. Rev. B* **58** 2482 (1998)
35. Simak S I et al. *Phys. Rev. Lett.* **85** 142 (2000)
36. Hansen M, Anderko K *Constitution of Binary Alloys* (New York: McGraw-Hill, 1958) [Translated into Russian (Moscow: Metallurgizdat, 1962)]; reprinted (New York: Genium Publ. Corp., 1989)
37. Pearson W B *A Handbook of Lattice Spacings and Structures of Metals* Vol. 1 (New York: Pergamon Press, 1958)
38. Svechkarev I V *Zh. Eksp. Teor. Fiz.* **47** 960 (1964) [*Sov. Phys. JETP* **20** 643 (1965)]
39. Degtyareva O et al. *J. Phys.: Condens. Matter* **13** 7295 (2001)
40. Degtyareva V F et al. *J. Phys.: Condens. Matter* **15** 1635 (2003)
41. Olijnyk H, Holzapfel W B *J. Phys. Colloq.* (Paris) **45** C8-153 (1984)
42. Cheong B H, Chang K J *Phys. Rev. B* **44** 4103 (1991)
43. Degtyareva V F, Winzenick M, Holzapfel W B *Phys. Rev. B* **57** 4975 (1998)
44. Degtyareva V F et al. *Phys. Rev. B* **59** 6058 (1999)
45. Degtyareva V F et al. *Phys. Rev. B* **61** 5823 (2000)
46. Degtyareva O, Degtyareva V F *J. Phys.: Condens. Matter* **14** 407 (2002)
47. Benedict U et al. *J. Magn. Magn. Mater.* **29** 287 (1982); Haire R G et al. *Phys. Rev. B* **67** 134101 (2003)
48. Endo S, Sasaki H, Mitsui T *J. Phys. Soc. Jpn.* **42** 882 (1977); Olsen J S et al. *Physica B+C* **133** 129 (1985); McMahon M I, Nelmes R J *Phys. Rev. Lett.* **78** 3884 (1997)
49. Vohra Y K et al. *J. Appl. Phys.* **85** 2451 (1999)
50. Vohra Y K, Akella J *Phys. Rev. Lett.* **67** 3563 (1991)
51. Benedict U *J. Alloys Comp.* **223** 216 (1995); Shirotani I et al. *Physica B* **334** 167 (2003)
52. Degtyareva O et al. *Phys. Rev. Lett.* **93** 205502 (2004)
53. Mailhiot C, Grant J B, McMahan A K *Phys. Rev. B* **42** 9033 (1990); Bose S K, Kato T, Jepsen O *Phys. Rev. B* **72** 184509 (2005)
54. Eremets M I et al. *Science* **293** 272 (2001)
55. Tonkov E Yu *Fazovye Diagrammy Elementov pri Vysokom Davlenii* (Phase Diagrams of Elements under High Pressure) (Moscow: Nauka, 1979)
56. Jayaraman A et al. *J. Phys. Chem. Solids* **24** 7 (1963)
57. Tonkov E Yu, Ponyatovsky E G *Phase Transformations of Elements Under High Pressure* (Advances in Metallic Alloys, Vol. 4) (Boca Raton, Fla.: CRC Press, 2005)
58. Neaton J B, Ashcroft N W *Nature* **400** 141 (1999)
59. Degtyareva V F *High Press. Res.* **23** 253 (2003)
60. Degtyareva V F, in *High-Pressure Crystallography* (NATO Sci. Series, Ser. II, Vol. 140, Eds A Katrusiak and P McMillan) (Dordrecht: Kluwer Acad. Publ., 2004) p. 447
61. Shimizu K et al. *Nature* **419** 597 (2002)
62. Struzhkin V V et al. *Science* **298** 1213 (2002)
63. Deemyad S, Schilling J S *Phys. Rev. Lett.* **91** 167001 (2003)
64. Lin T H, Dunn K J *Phys. Rev. B* **33** 807 (1986)
65. Fortov V E et al. *Pis'ma Zh. Eksp. Teor. Fiz.* **74** 458 (2001) [*JETP Lett.* **74** 418 (2001)]
66. Rodriguez-Prieto A, Bergara A, cond-mat/0505619; Profeta et al. *Phys. Rev. Lett.* **96** 047003 (2006); Kasinathan D et al. *Phys. Rev. Lett.* **96** 047004 (2006)
67. Hanfland M et al., ESRF Annual Report HS-1839 (2002)
68. Gregoryanz E et al. *Phys. Rev. Lett.* **94** 185502 (2005)
69. Ross M, McMahan A K *Phys. Rev. B* **26** 4088 (1982)
70. Wittig J, in *High Pressure in Science and Technology: Proc. of the IX AIRAPT Intern. Conf., Albany, New York, USA, July 24–29, 1983* (Materials Research Soc. Symp. Proc., Vol. 22, Eds C Homan, R K MacCrone, E Whalley) (New York: North-Holland, 1984) p. 17
71. Takemura K, Minomura S, Shimomura O *Phys. Rev. Lett.* **49** 1772 (1982)
72. Olijnyk H, Holzapfel W B *Phys. Lett. A* **99** 381 (1983)
73. Schwarz U et al. *Solid State Commun.* **112** 319 (1999)
74. Takemura K et al. *Phys. Rev. B* **62** R10603 (2000)
75. Degtyareva V F *Phys. Rev. B* **62** 9 (2000)
76. Degtyareva V F, Degtyareva O, Allan D R *Phys. Rev. B* **67** 212105 (2003)
77. Wittig J *Phys. Rev. Lett.* **24** 812 (1970)
78. Ullrich K, Berichte Kernforschungsanlage Jülich JUEL-1634 (1980) p. 1
79. Erskine D et al. *Phys. Rev. Lett.* **57** 2741 (1986)
80. Rabin'kin A G, Laukhin V N *Zh. Eksp. Teor. Fiz.* **61** 642 (1971) [*Sov. Phys. JETP* **34** 342 (1972)]
81. Laukhin V N *Fiz. Tverd. Tela* **16** 2765 (1974) [*Sov. Phys. Solid State* **16** 1792 (1974)]
82. Laukhin V N, Matyushchenkov V K, Rabin'kin A G *Fiz. Tverd. Tela* **16** 276 (1974) [*Sov. Phys. Solid State* **16** 183 (1974)]
83. Olijnyk H, Holzapfel W B *Phys. Lett. A* **100** 191 (1984)
84. McMahon M I et al., ESRF Annual Report HS-2303 (2003)
85. Allan D R et al. *Rev. High Pressure Sci. Technol.* **7** 236 (1998)
86. Bovornratanaraks T et al. *Phys. Rev. B* **73** 144112 (2006)
87. Karuzawa M, Ishizuka M, Endo S *J. Phys.: Condens. Matter* **14** 10759 (2002)
88. Chen A L et al. *Phys. Rev. B* **46** 5523 (1992)
89. Okada S et al. *J. Phys. Soc. Jpn.* **65** 1924 (1996)
90. Dunn K J, Bundy F P *Phys. Rev. B* **24** 1643 (1981); Yabuuchi T et al. *J. Phys. Soc. Jpn.* **74** 2391 (2005)

91. Fortov V E et al. *Pis'ma Zh. Eksp. Teor. Fiz.* **79** 425 (2004) [*JETP Lett.* **79** 346 (2004)]
92. Bireckoven B, Wittig J, in *High Pressure in Science and Technology: Proc. of the XI AIRAPT Intern. Conf., Kiev, USSR, 12 – 17 July 1987* (Kiev: Naukova Dumka, 1989) p. 14
93. Andersson G, Sundqvist B, Bäckström G *J. Appl. Phys.* **65** 3943 (1989)
94. Brandt N V, Ginzburg N I *Zh. Eksp. Teor. Fiz.* **39** 1554 (1960) [*Sov. Phys. JETP* **12** 1082 (1961)]
95. Wittig J *J. Phys. Chem. Solids* **30** 1407 (1969)
96. Wittig J, Matthias B T *Phys. Rev. Lett.* **22** 634 (1969)
97. Probst C, Wittig J *Phys. Rev. Lett.* **39** 1161 (1977)
98. Shimizu K, Amaya K, Suzuki N *J. Phys. Soc. Jpn.* **74** 1345 (2005)
99. Akahama Y, Fujihisa H, Kawamura H *Phys. Rev. Lett.* **94** 195503 (2005)
100. Fujihisa H et al. *Phys. Rev. B* **72** 132103 (2005)
101. Wittig J et al. *Phys. Rev. Lett.* **42** 469 (1979)